FINAL REPORT

Title: *Novel Anionic Clay Adsorbents for Boiler-Blow Down Waters Reclaim and Reuse*

Type of Report: *Final*

Reporting Period Start Date: *9/01/04*

Reporting Period End Date: *8/31/05*

Principal Authors: *Muhammad Sahimi and Theodore T. Tsotsis*

Date Report was Issued: *December 2005*

Name and Address of Submitting Organization: *Mork Family Department of Chemical Engineering and Materials Science, Viterbi School of Engineering, University of Southern California, Los Angeles, CA 90089-1211*

ABSTRACT

Our goal in this study is to utilize novel anionic clay sorbents for treating and reclaiming/reusing power-plant effluents, in particular, boiler blow-down waters containing heavy metals, such as As and Se. Developing and using novel materials for such application is dictated by the challenge posed by reclaiming and recycling these "too clean to clean" effluent streams, generated during electricity production, whose contaminant levels are in the ppm/ppb (or even less) trace levels. During the study model blow-down streams have been treated in batch experiments. Adsorption isotherms as a function of pH/temperature have been established for both As and Se. Adsorption rates have also measured as a function of concentration, temperature, pH, and space time. For both the equilibrium and rate measurements, we have studied the As/Se interaction, and competition from background anions. A homogenous surface diffusion model is used to describe the experimental kinetic data. The estimated diffusivity values are shown to depend on the particle size. On the other hand, a model taking into account the polycrystalline nature of these adsorbent particles, and the presence of an intercrystallite porous region predicts correctly that the surface diffusivity is particle size independent. A mathematical model to describe flow experiments in packed-beds has also been developed during phase I of this project. The goal is to validate this model with flow experiments in packed-beds during the phase II of this project, to determine the adsorption capacity under flow conditions, and to compare it with the capacity estimated from the adsorption isotherms determined from the batch studies.

TABLE OF CONTENTS

1. Executive Summary

1.1 Objectives

U.S. electric utilities are a large user of water. New regulations to diminish the effect of power generation on aquatic life will mean, that Utilities will have to retrofit from the once-through cooling technology, to recirculating cooling towers, and to reclaim/reuse discharged water throughout the power-plant (e.g., boiler blow-down water). Concerns exist today, in particular, about heavy metals, such as Hg, As and Se, found in many of the power-plant effluents. Most of these streams fall today under the category of high volume, "too clean to clean" effluents. They require highly efficient treatment techniques, particularly for the removal of trace-level metal contaminants. Little emphasis, so far, has been placed on such discharges. The focus of this project is on treating and reusing such effluents, particularly on dealing with Se and As impacted boiler blow-down streams. Our goal is to study the utilization of novel anionic clay sorbents for treating and reclaiming/reusing power-plant effluents, in particular, boiler blow-down waters containing heavy metals, such as As and Se. Developing and using novel materials for such application is dictated by the challenge posed by reclaiming and recycling these "too clean to clean" effluent streams, generated during electricity production, whose contaminant levels are in the ppm/ppb (or even less) trace levels. This is an exploratory project combining the expertise of three uniquely qualified groups USC, M&PT and GCSC.

1.2 Project Accomplishments

At the start of the project, we contacted a number of utilities in the Southern California region identified in collaboration with the GCSC and various State Agencies. Two utilities (Harbor Co-generation Station and the Redondo Generating Station) were selected and waste-water samples from these two utilities were collected and analyzed for their metal content (including As and Se) using ICP-MS. In addition to our own analysis of these two sites, we received further information about effluents from various power plants in our state and elsewhere. All the various sources of data indicate the presence of As and Se in power plant discharges, usually in small concentrations up to 50 ppb. Based on these findings model effluent streams containing from 20-200 ppb of As and Se were generated in order to study the removal of metals using anionic clay materials.

These model blow-down streams have been treated in batch experiments at the relevant blow-down stream temperatures. Adsorption isotherms as a function of pH/temperature have been established for both As and Se. Upon completion of the equilibrium studies, emphasis shifted to the measurement of rates (as they also impact design, adsorber service life, and process viability), using ground adsorbent particles, to eliminate transport limitations that may falsify the data. The rates are measured as a function of concentration, temperature, pH, and space time. Similarly with the equilibrium measurements, we have studied the As/Se interaction, and competition from background anions

In parallel with the sorption experiments, we have carried out research to understand what determines sorbent selectivity. In particular, the emphasis has been on the effect of adsorbent particle size, as it is critical in determining column performance. Conditioning the adsorbent

significantly reduced the dissolution previously observed with uncalcined and calcined LDH. The adsorption rates and isotherms have been investigated in batch experiments. As(V) adsorption is shown to follow the Sips adsorption isotherm. The As(V) adsorption rate on conditioned LDH increases with decreasing adsorbent particle size; the adsorption capacity of As(V) on conditioned LDH, on the other hand, is independent of particle size. A homogenous surface diffusion model is used to describe the experimental kinetic data. The estimated diffusivity values are shown to depend on the particle size. On the other hand, a model taking into account the polycrystalline nature of these adsorbent particles, and the presence of an intercrystallite porous region predicts correctly that the surface diffusivity is particle size independent.

1.3 Future Work

A mathematical model to describe flow experiments in packed-beds has also been developed during phase I of this project. The goal is to validate this model with flow experiments in packed-beds during the phase II of this project, to determine the adsorption capacity under flow conditions, and to compare it with the capacity estimated from the adsorption isotherms determined from the batch studies.

These experiments will be coupled with simulations of the sorbent structure, and its interactions with oxyanions of interest. The combined simulation and experimental studies will provide insight into how the existing sorbents work, and guidance in the development of 2nd generation sorbents during the phase II of this project.

2.   REPORT DETAILS

2.1 Introduction and Research Approach

Arsenic, which is toxic to humans and other living organisms, presents potentially a serious environmental problem throughout the world [Basu *et al*., 2001]. Arsenic usually occurs as arsenate [As(V)] or arsenite [As(III)] in potable water supplies. The type of arsenic species found in water depends on its pH and redox potential [Massechelyen *et al*., 1991]. Arsenate (H_3AsO_4, $H_2AsO_4^-$, $HAsO_4^{2-}$, AsO_4^{3-}) is typically present in the mono-and divalent anionic forms in oxygenated waters, while arsenite (H_2AsO_3, $H_2AsO_3^-$, and $HAsO_3^{2-}$) occurs primarily in the neutral form in lower redox potential waters [Smedley *et al*., 2002]. The maximum contaminant level (MCL) for arsenic in drinking water in Europe, Japan, and the USA (starting 2006) is 10μg /l. As a result of establishing of this lower MCL, there is an increased need for arsenic removal processes suitable for treating water sources with low ambient arsenic concentrations; adsorption processes using layered double hydroxide (LDH) materials have proven promising in this regard [Yang *et al.,* 2005].

U.S. electric utilities are a large user of water. New regulations to diminish the effect of power generation on aquatic life will mean that Utilities will have to retrofit from the once-through cooling technology, to recirculating cooling towers, and to reclaim/reuse discharged water throughout the power-plant (e.g., boiler blow-down water). Concerns exist today, in particular, about heavy metals, such as Hg, As and Se, found in many of the power-plant effluents. Most of these streams fall today under the category of high volume, "too clean to clean" effluents. They require highly efficient treatment techniques, particularly for the removal of trace-level

metal contaminants. Little emphasis, so far, has been placed on such discharges. The focus of this project is on treating and reusing such effluents, particularly on dealing with Se- and As-impacted boiler blow-down streams. Our goal is to study the utilization of novel anionic clay sorbents for treating and reclaiming/reusing power-plant effluents, in particular, boiler blow-down waters containing heavy metals, such as As and Se. In particular, our objectives are:

1) To undertake the identification, sampling, and analysis of boiler blow-down effluents and discharges from selected local electric utilities. The goal here is to establish "typical" contaminant profiles of such streams.

2) Using a number of "surrogate" boiler blow-down streams to perform preliminary reclaim/reuse studies focusing on anionic clay materials, namely calcined and uncalcined layered double hydroxides (LDH). The goal here is to establish a preliminary treatability database using the layered double hydroxides, and to investigate how suitable these adsorbents are for a given stream application.

For objective #1, our approach was to seek to establish a database using information obtained from selected utilities. Considerable amount of information was found, for example, in a report by the Southern California Coastal Water Research Project for the year 2000, which contained effluent data from 13 power generating stations located on the Southern California Coast. We also obtained water samples from two selected power plants to perform a comprehensive composition analysis in order to identify:

- Soluble As and Se; these were determined by inductively coupled plasma mass spectrometry

(ICP-MS, Perkin-Elmer ELAN-9000) following the methodology of EPA method 200.8 and EPA method 1638 (this method does not determine the oxidation state of the metals).

- Other metals present; these were also profiled using an ICP-MS scan.

For objective #2, "model" blow-down streams were generated representing the maximum, minimum or average levels of As and Se contaminants and pH range based upon the study conducted in objective #1. The water samples were then treated in batch experiments using LDH. The goals of these experiments were:

- To establish the adsorption isotherms as a function of pH and temperature for both As and Se in the concentration range of interest. The effect of the As and Se oxidation state on the adsorption was to be studied as well.

- To study the adsorption kinetics for the adsorption of As and Se on both calcined and uncalcined LDH, since such kinetics are important for estimating adsorber service life, and for optimal adsorber design.

- To determine potential capacity reduction as a result of competition by background ions, such as CO_3^{2-}, SO_4^{2-}, NO_3^{-} and HPO_4^{2-}.

- To study the desorption properties of the LDH adsorbents.

Magnesium-aluminum-carbonate-LDH (Mg-Al-CO$_3$-LDH) was used for the adsorption experiments. The adsorbents were prepared by the co-precipitation method, following a method proposed by Jules *et al*. (2002). The calcined Mg-Al-LDH was obtained by heating the original (referred to as uncalcined) LDH in a muffle furnace at 773 K for 4 h in an air atmosphere with

heating and cooling rates of 2 K·min^{-1}. Batch adsorption studies were performed at various temperatures in order to obtain the equilibrium adsorption isotherms. Aqueous solutions of As(V) and Se(IV) of a pre-determined concentration ranging from 20 ppb to 200 ppb were prepared by diluting 1000 ppm ICP standard solutions. The initial pH of these solutions ranged from 4.2 to 5.4. No pH adjustment was carried out in order to avoid any possible interference of foreign anions during the adsorption process. For these experiments, a constant mass of the LDH was added to a 13 ml snap-seal polyethylene bottle, which was then filled with a 10 ml aqueous solution of As or Se of a given concentration. The bottles containing the LDH suspension and the As and Se solutions were kept closed for the whole period of the adsorption experiment. They were placed in a reciprocal shaking water-bath (Precision Model 25) and were shaken at 150 rpm (rotations per minute) for 24 h in order for the adsorption on the LDH to reach equilibrium. The mixture in each bottle was then centrifuged immediately, and the As and Se concentrations in the supernatant solutions were determined by ICP-MS (Perkin-Elmer ELAN-9000). For the experiments measuring the adsorption kinetics, the solutions were prepared by the addition of 90 mg of LDH to 750 ml of 20 ppb As or Se solutions in a 1 L screw-top bottle. During the experiments, the mixture was shaken at 150 rpm at a predetermined temperature, and at selected time intervals 4ml samples were extracted, centrifuged, and the As or Se concentrations were determined by ICP-MS.

To investigate the effect of competing ions, the LDH were accurately weighed and added to 10 ml of 20 ppb As or Se solutions containing additional competing ions, such as NO_3^-, CO_3^{2-},

SO_4^{2-} and HPO_4^{2-}, with various concentrations; these were prepared using $NaNO_3$, Na_2CO_3, Na_2SO_4 and K_2HPO_4, respectively. The samples were shaken for 24 h and centrifuged; the concentrations of As or Se still remaining in solution were then determined.

Desorption experiments were conducted, in which the effects of using different desorption solutions containing various anions, with concentrations ranging from 100 ppb to 1000 ppm were investigated. Initially, 10 ml of 20 ppb As or Se solutions were equilibrated with the calcined LDH, as described above. After centrifuging, 4 ml of the equilibrated solution were removed for the ICP-MS analysis, and were substituted by 4 ml of the solution containing other anions (e.g., NO_3^-, CO_3^{2-}, SO_4^{2-}, HPO_4^{2-}); the resulting solution was then shaken for an additional 2 h and centrifuged again. Four ml of the supernatant solution were then again substituted by 4 ml of the solution containing the other anions, and the process was repeated; the overall desorption experiment consisted of five such dilution cycles.

The ICP-MS detection limit was found to be 0.043 µg/l for arsenic and 0.172 µg/l for selenium using the EPA 200.8 method. Experimental errors were checked randomly for some of the experiments. The experimental errors were all within ±3%. We repeated many of the experiments on the adsorption and desorption kinetics, isotherms, and the effect of pH. All of them showed good repeatability. Analysis of duplicate experiments found the variability to be within ±8%.

2.2   Results and Discussion

2.2.1 The As and Se concentrations in power-plant effluent streams were determined.

We completed all tasks related to objective #1. With assistance from our colleagues from the Southern California Gas Company we developed contacts with the Southern California Coastal Water Research Project (SCCWPR), the Department of Water and Power (DWP), as well as the Regional Water Board (RWB), all of which provided us a wealth of information about the effluents from various power plants in California and elsewhere. We received the recently generated report on "Characterization of Effluents from Power Generating Stations in the Southern California Bight in 2000," [Steinberger and Stein 2004], which provides useful data about the Se and As concentrations in the effluents from power-plants in the Southern California region. In addition, we visited the Harbor Co-generation Station, and the Redondo Generating Station, where we obtained several effluent samples and analysis reports. The concentration of As and Se in these effluents were analyzed in our laboratories using ICP-MS analysis. Thus, we were able to establish "typical" contaminant profiles of these streams and to create "surrogate" boiler blow-down effluents to perform preliminary reclaim/reuse studies focusing on calcined and uncalcined layered double hydroxides.

2.2.2 The removal of As and Se from model boiler blow-down streams on calcined and uncalcined layered double hydroxides was studied.

We completed all tasks relevant to objectives #2 above. The following discussion summarizes key technical findings:

2.2.2.1 Characterization of the calcined and uncalcined LDH

FT-IR spectra of the calcined and uncalcined LDH in the room environment are shown in Figure

1. The broad absorption peak in the uncalcined LDH spectra (see Figure 1 a) between 3600 and 3300 cm^{-1} is due to the vibration of structural OH^{-} groups from the brucite-like layers. The peaks around 1655 and 3038 cm^{-1} are due to the interlayer water molecules. The peaks around 1377, 874 and 685 cm^{-1} are due to the carbonate ions. FT-IR spectra of calcined LDH suggest that most of the interlayer water bands have disappeared, but some of the carbonate anions are still present after calcination (e.g., bands at around 1389 cm^{-1} in Figure 1b). These may also be due, however, to the carbonate species adsorbed when the LDH sample is cooling in the atmosphere during the calcination.
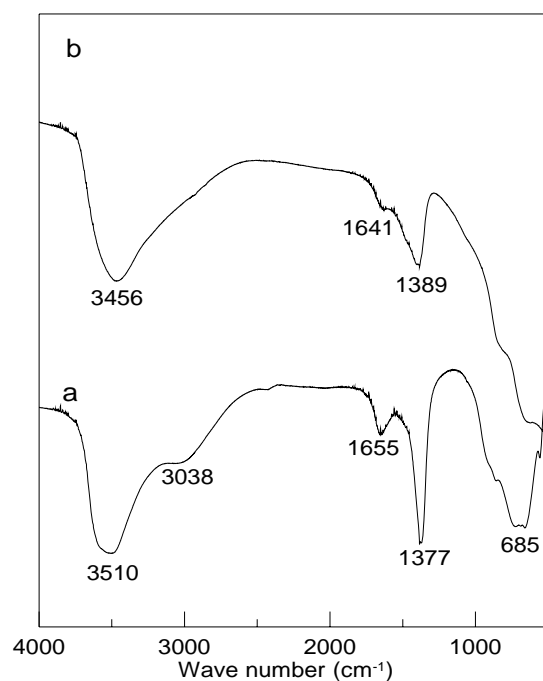
Figure 1. FT-IR spectra of (a) LDH and (b) calcined LDH

The specific surface areas of uncalcined and calcined LDH were determined by the single-point BET method, and were found to be 47 and 198 m^2/g, respectively. That the calcined-LDH has the higher surface area, has also been previously reported by other

investigators, and is believed to be due to the additional mesoporous region which is created by

the formation of channels and pores resulting from the removal of water and carbon dioxide

[Reichle *et al.,* 1986].

2.2.2.2 Batch experiments

●   **As(V) has a greater adsorption affinity than Se(IV) for both calcined and uncalcined**

 LDH. The adsorption capacities of As(V) and Se(IV) on the calcined LDH are higher

 **than those on the uncalcined LDH.**

Adsorption processes are usually modeled by different types of isotherms, (Freundlich, Langmuir,

Sips, et.). Figure 2 shows the adsorption isotherms generated in the batch experiments together

with their fit to the calculated Freundlich adsorption isotherm (in the form

$log(q_e)=logK+1/nlog(C_e)$, where q_e is the amount of solute adsorbed at equilibrium, and C_e is the

bulk concentration of the solute).

Table 1.   Freundlich adsorption constants for the adsorption of As and Se on LDH

	K	$1/n$	R^2
As/calcined LDH	136.1	0.884	0.972
Se/calcined LDH	19.22	0.923	0.990
As/uncalcined LDH	57.29	0.683	0.991
Se/uncalcined LDH	3.48	1.133	0.997

The data show a satisfactory fit to the Freundlich isotherm (better than the fit to the Langmuir

isotherm equation -- a different type of two-parameter isotherm, namely the Sips isotherm also

satisfactorily fits the experimental data, see further discussion in the report), with an R^2 greater

than 0.97 (R^2 is the coefficient of determination, and expresses the amount of common variation

between the two variables).
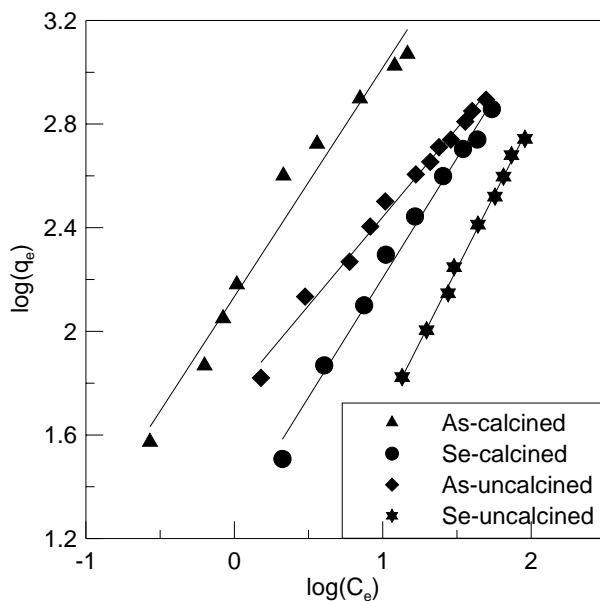
Figure 2. Adsorption isotherms for As(V) and Se(IV) on calcined and uncalcined LDH.

The estimated K [(mg solute/kg adsorbent) $\cdot$(l/μg solute)$^{1/n}$] and n values are shown in Table 1.

In the Freundlich isotherm model, K is a measure of the adsorption capacity (larger K indicates a

larger overall capacity), whereas the parameter $1/n$ is a measure of the strength of adsorption

(larger n indicates higher adsorption affinity). As can be seen in Table 1, As(V) has a larger

adsorption capacity than Se(IV) for both the uncalcined and calcined LDH. The isotherms also

indicate that the adsorption capacity of As(V) and Se(IV) on the calcined-LDH is considerably

higher than that on the uncalcined LDH. The higher adsorption capacity on calcined LDH is

explained by the loss of H_2O and CO_3^{2-} due to calcination, resulting in a higher anion exchange

capacity, and the higher surface area resulting from calcination.

- **An mth order kinetic rate equation describes well the adsorption kinetic of As and Se on calcined and uncalcined LDH.**

The adsorption of As(V) and Se(IV) from aqueous solutions on calcined LDH is a relatively fast process (compared to the uncalcined LDH), and equilibrium for the 20 ppb solutions is obtained within the first 2 h of adsorption. Se(IV) adsorption on the uncalcined LDH is also a rather fast process, and reaches equilibrium within 2 h. Adsorption of As(V) on uncalcined LDH is a slow process, however, and reaches equilibrium only after a 24 h reaction time. Adsorption kinetics models correlate the solute uptake rate with bulk concentration of the solute to be adsorbed; these models are important in water treatment process design and optimization. To fit the experimental data, we have utilized an mth order kinetic rate equation of the form (a different but equivalent approach to model the batch reaction data has also been utilized, see section 5.2..3 below):

$$dq_t / dt = k_1 (q_e - q_t)^m \tag{1}$$

where q_e is the amount of solute adsorbed (mg solute/kg adsorbent) at equilibrium with the corresponding bulk concentration of the solute, q_t the amount of solute adsorbed on the LDH at any time, m is the adsorption rate order, and k_1 is the effective adsorption rate constant. Equation 1 must be coupled with the mass balance equation below for the batch reactor system

$$V \frac{dC}{dt} = -W \frac{dq_t}{dt} \tag{2}$$

where C is the bulk concentration for the solute (µg/l) at time t, V (ml) the volume of the reactor, and W (mg) the amount of the adsorbent present. Equations 1 and 2 must also be coupled with the

Freundlich adsorption equilibrium relationship (see discussion below)

$$q_e=KC^{1/n} \tag{3}$$

A Genetic Algorithm which uses selection, crossover and mutation steps to update the parameter values is utilized to calculate the values of parameters, which are consistent with the experimental data. Figure 3 shows the raw experimental data for As(V) and Se(IV) on calcined or on uncalcined LDH in the form of the concentration remaining in the solution versus time together with the calculated theoretical lines based on the estimated parameter values. The estimated values of the model parameters (k_1 and m) together with the corresponding coefficients of determination R^2 are shown in Table 2.

Table 2. Kinetic parameters for the adsorption experiments

	k	m	R^2
As/calcined LDH	1.53 E-5	2.01	0.988
Se/calcined LDH	3.12 E-3	1.49	0.986
As/uncalcined LDH	1.86 E-5	2.01	0.933
Se/uncalcined LDH	4.69 E-4	2.01	0.903

● **The starting solution pH does not significantly influence the adsorption of As and Se on**

calcined LDH, as long as it is higher than 4; As and Se adsorption on uncalcined LDH is, however, more sensitive to variations in the initial pH.

The amounts of As(V) and Se(IV) adsorbed on calcined LDH (Figure 4a) decrease with decreasing pH, for starting solution pH below 4; for pH above 4, the adsorption seems to be pH-independent. The decrease in adsorption with decreasing pH in the low pH range may be due to the dissolution of LDH in the low pH solutions. This was confirmed by the presence of magnesium (Mg) and aluminum (Al) in the final solution using the ICP-MS analysis. The adsorption of As (V) and Se (IV) on uncalcined LDH shows a different behavior with respect to the starting

(a)　　　　　　　　　　　　　　(b)
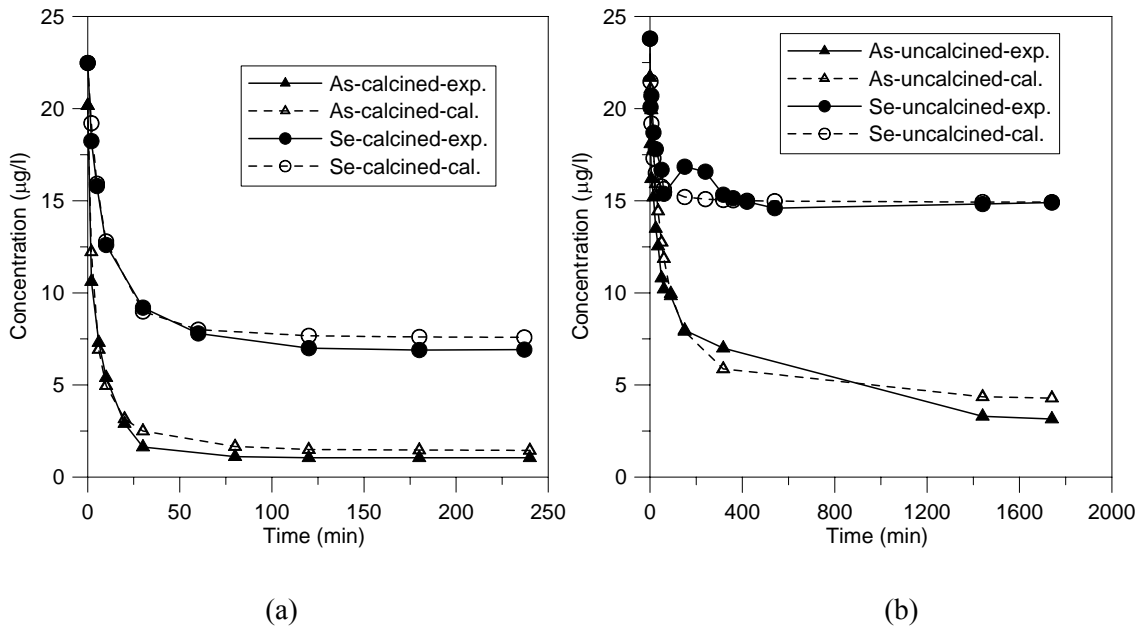
Figure 3. Comparison between the measured and modeled time profiles for adsorption of As and Se on (a) calcined and (b) uncalcined LDH.

solution pH than the adsorption on the calcined LDH. As Figure 4b indicates, there is a certain

range of pH values for which the adsorbed amount is maximized. For As(V), adsorption is fairly

high in a starting pH range from 5-8. Below pH 5, adsorption decreases sharply with decreasing

pH (this again may due to the dissolution of the LDH structure), and the same is true with

increasing pH above 8 (see explanation below). Adsorption of Se(IV) on uncalcined LDH first

increases with increasing pH, and reaches its maximum at ~ pH 4. Then, the adsorption decreases,

and appears to reach a plateau in the pH range of 6-8; the adsorption decreases again with

increasing pH, above 8.

(a)   (b)
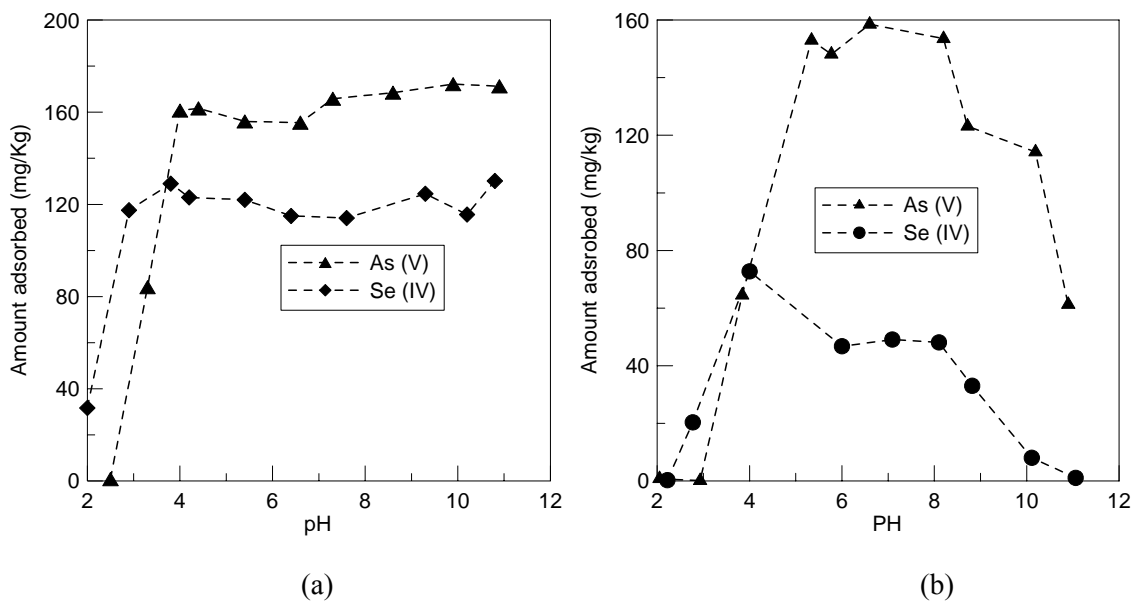
Figure 4.   The effects of *pH* on the uptake of As(V) and Se(IV) in 20 ppb solutions on (a)

calcined and (b) uncalcined LDH.

The effect of pH on adsorption on uncalcined LDH can be explained in the region of high pH

by the effect of pH on the point of zero charge (pH_{pzc}), which for the uncalcined LDH was

reported to be in the range 6.8-8.9 [Das *et al*., 2003; Manju, 1999]. The surface of LDH is

negatively charged when pH>pH$_{pzc}$. Therefore, in the higher pH range, the arsenate and selenite

anionic species will be repelled by the LDH surface. The negative effect of pH may be further

compounded by the increasing competitive effect of OH$^-$ adsorption in the higher pH range. For

pH<pH$_{pzc}$ the LDH surface is positively charged, which is normally beneficial for the adsorption

of the negatively charged anionic species. On the other hand, as previously noted, very low pH

negatively impacts the stability of the LDH structure.

- **As(III) is more difficult to remove than As(V) by both the calcined and uncalcined LDH.**

  Calcined LDH have a larger adsorption capacity for Se(IV) than Se(VI), whereas Se(VI)

  adsorption is significantly greater than Se(IV) on uncalcined LDH.

As(III) adsorbs less from aqueous solutions than As(V) (Figure 5); in fact, uncalcined LDH

adsorbs almost no As(III). The difference in the total amounts of As(III) and As(VI) adsorbed on

the LDH adsorbents may be related to the different species found in solution for these two forms

of As with a different oxidation state. Arsenate is present as negatively charged ionic species

(either H$_2$AsO$_4^-$ or HAsO$_4^{2-}$) in a broader range of pH conditions than arsenite, which is mostly

found in the non-ionic form (H$_3$AsO$_3$) [Smedley *et al*., 2002]. The negatively-charged As(V)

species are expected to be more easily adsorbed by the LDH structure, either through anion

exchange for the uncalcined LDH, or by rehydration and incorporation into the calcined LDH, in

order to rebuild the initial LDH structure. For selenium, calcined and uncalcined LDH show

different adsorption behavior towards Se (IV) and Se (VI) (Figure 6).
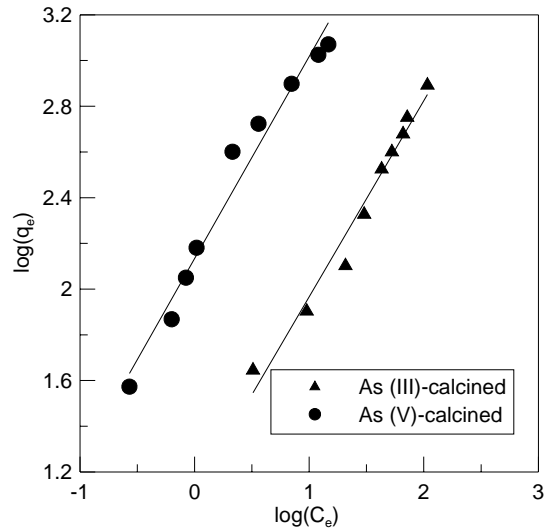
Figure 5. Adsorption isotherms of As(III) and As(V) on calcined LDH

On the calcined LDH, Se (IV) is adsorbed in larger amounts than Se(VI), whereas Se(VI) adsorption is greater than Se(IV) on uncalcined LDH. Differences in the adsorption characteristics between Se(IV) and Se (VI) were also previously reported by other investigators. Kuan *et al*. [1998] reported, for example, selenium adsorption in surface coal-mine soils. The adsorption of Se(VI) was shown to be stronger than that of Se(IV). Saviz and David [1998]] reported that Se(VI) exhibits higher affinity towards the surface of activated alumina, and was, therefore, more easily removed than Se(IV), except for pH >6.

● **Competing ions have a greater effect on Se(IV) rather than on As(V) uptake.**

NO_3^- ions have almost no effect on the adsorption of As(V) on the calcined LDH up to a concentration of 1000 ppm (50,000 times higher than the initial concentration of As(V) of 20 ppb), see Figure 7a**.** SO_4^{2-} and CO_3^{2-} have a modest effect, causing only 14% and 20% reductions when their concentration is 500 ppm, and 33% and 45% reductions, respectively, when the concentration is 1000 ppm. HPO_4^{2-} appears to be the anion that most negatively impacts

adsorption of As(V). When its concentration is 20 ppm, adsorption of As is 34% less than when

HPO_4^{2-} is absent from the solution. As(V) adsorption completely stops when the HPO_4^{2-}

concentration is higher than 500 ppm. To summarize, the effect of competing anions on

adsorption of As(V) decreases in the order: $HPO_4^{2-} > CO_3^{2-} \sim SO_4^{2-} > NO_3^{-}$.
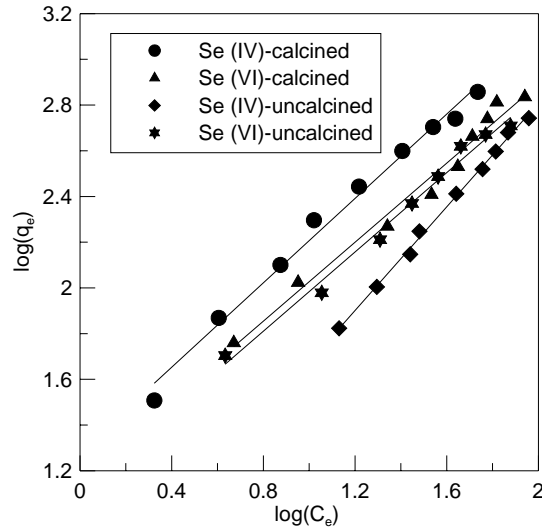
Figure 6. Adsorption isotherms of Se(IV) and Se(VI) on calcined and uncalcined LDH.

(a)   (b)
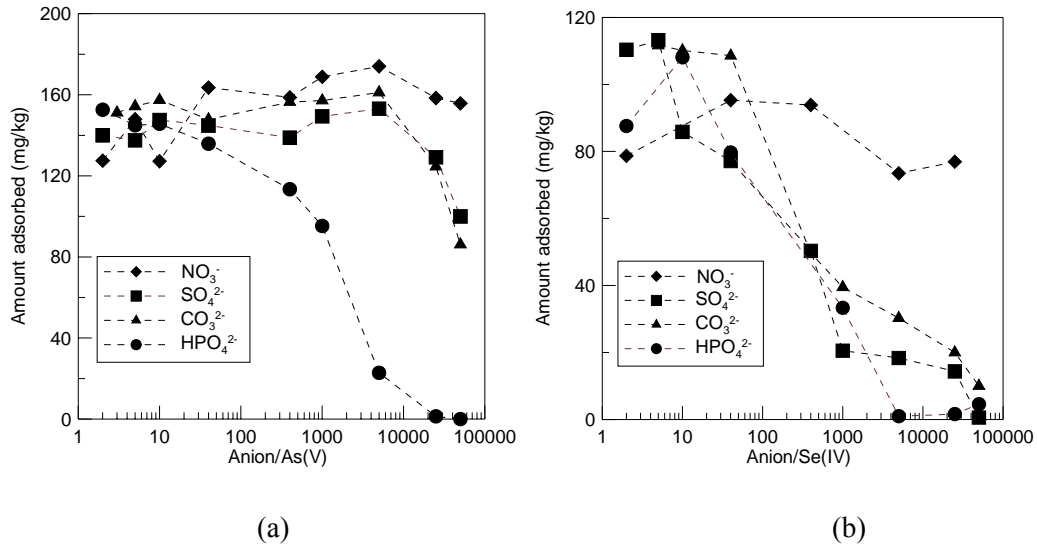
Figure 7. The effect of competitive anions on the uptakes of (a) As(V) and (b) Se(IV) on calcined

LDH in 20 ppb solutions.

Competitive anions have a stronger effect on Se(IV) uptake than on As(V), see Figure 7b. CO_3^{2-} and HPO_4^{2-} have significant effect on Se uptake, even when their concentrations are only 400 times higher than that of Se. The effect of competing anions on adsorption of Se (IV) decreases in the order $HPO_4^{2-} > SO_4^{2-} \sim CO_3^{2-} > NO_3^-$. However, in the case of Se the negative impact of HPO_4^{2-} is not as significantly different from that of carbonate and SO_4^{2-} as in the case of As(V). The differences in behavior between As(V) and Se(IV) on the effect of competitive ions are consistent with the differences in their adsorption affinities (see Table 1) towards the LDH.

- **The desorption of As(V) and Se(IV) from the LDH depends on the type of ion species present in the desorbing solutions, and their concentration.**

Figure 8 shows the effect of solutions containing various anions with differing concentration on the desorption of As(V) from calcined LDH. In the NO_3^- solution, only up to 17 % of the adsorbed As(V) is desorbed after 5 desorption cycles. For the CO_3^{2-} and SO_4^{2-} solutions, when above 10 ppm, the fraction of As(V) that desorbs increases with increasing carbonate and SO_4^{2-} concentration. After five cycles with the 1000 ppm CO_3^{2-} and SO_4^{2-} solutions, for example, 46% and 43% of As(V) are desorbed, respectively. The release of As(V) in HPO_4^{2-} solutions is faster, and more concentration-dependent. Almost 84 % of As(V) desorbs in the 100 ppm HPO_4^{2-} solution after the 5 desorption cycles. The desorption results for As(V) in the presence of various anions are consistent with the adsorption behavior in the presence of the same competitive anions.

We have found previously that the effect of various competitive anions on the adsorption of As on calcined LDH decreases in the order, $HPO_4^{2-} > CO_3^{2-} > SO_4^{2-} > NO_3^-$; we noted in the discussion that the reason for such a behavior is most likely the different affinities of the same
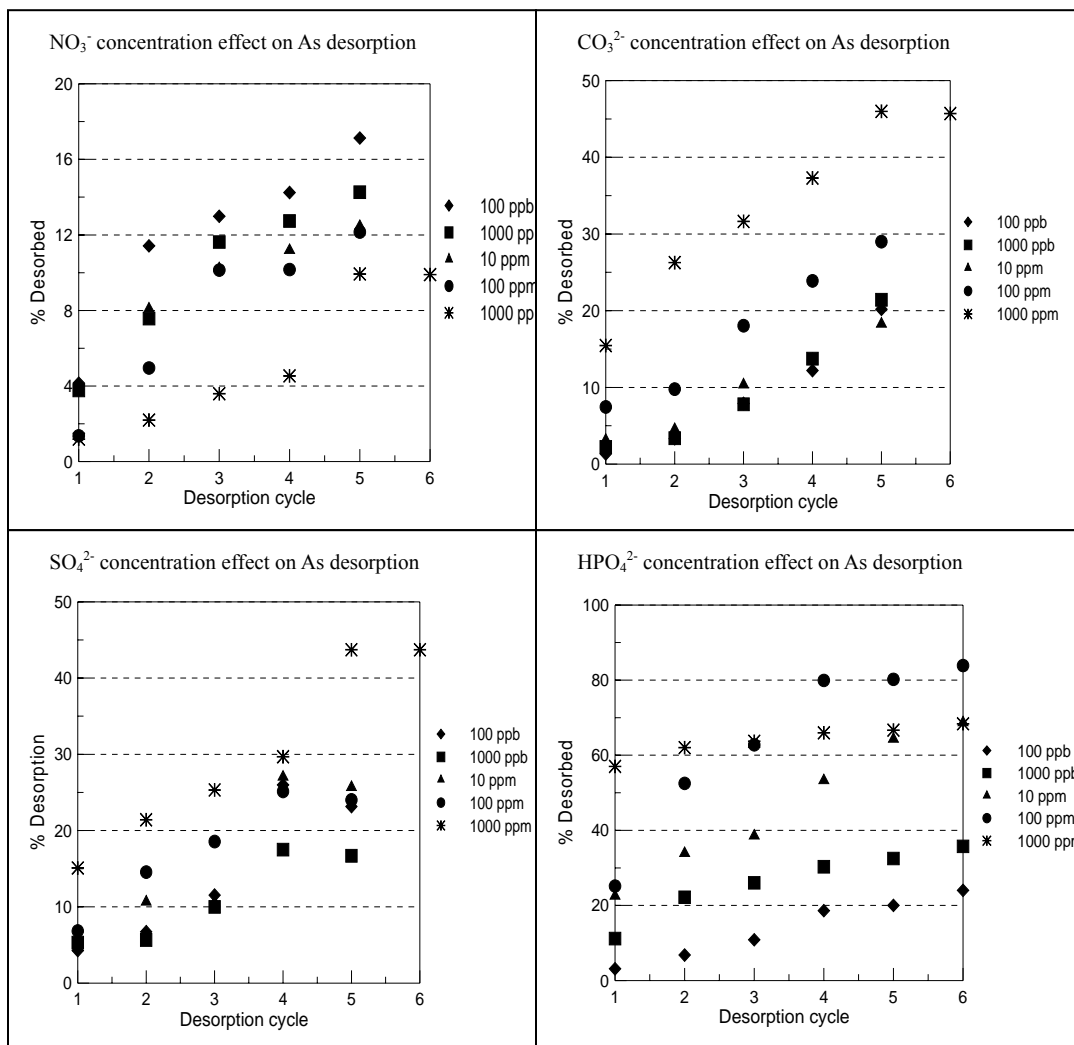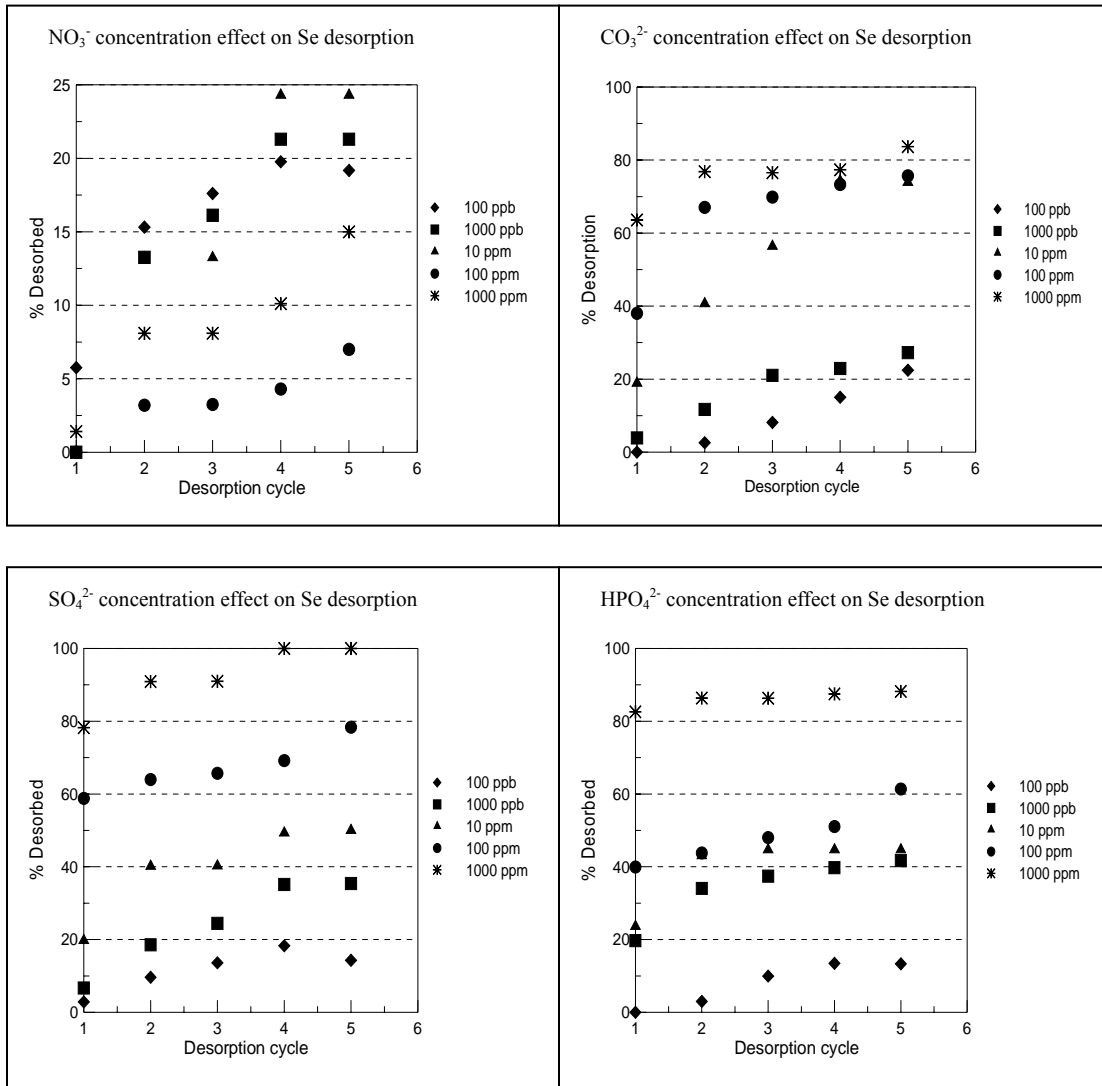
Figure 8. Desorption of As(V) from calcined LDH as a function of different anions.

anions for the LDH, which also follow the same order. As Goswamee *et al.* [1998] noted, when

an anion is better suited stereochemically for inclusion into the interlayer of LDH, it also has a

greater ability to cause the release of interlayer anions already present in the LDH.

Desorption of Se as a function of various anions and concentrations is shown in Figure 9.

Both the desorption rate and the fraction of Se(IV) that is desorbed from the calcined LDH are

higher than in the case of As(V). This behavior is consistent with the lower sorption affinity of Se

Figure 9. Desorption of Se(IV) from calcined LDH as a function of different anions.

towards the calcined LDH, since the lower the affinity of a given metal is to the calcined LDH,

the easier it is for the same metal to be released in the solution. In general, the release rates and

the fraction of Se metal removed in HPO_4^{2-}, SO_4^{2-}, and CO_3^{2-} solutions increase with an increase

in their concentrations. The maximum amount of desorption of Se is found in the 1000 ppm SO_4^{2-}

solution, for which 100% of adsorbed Se is desorbed.

2.2.3. The effect of particle size, and alternate approach for modeling the adsorption data

As noted above, LDH are potentially good adsorbents for a diverse number of anions because they offer a large interlayer surface to host these species, with the additional advantage that they can be easily recycled [Cavani *et al.,* 1991]. As detailed in our report, so far, we have investigated these materials in the removal of trace level of arsenic (and selenium) from aqueous solutions [Yang *et al*., 2005]. They were shown to be efficient adsorbents for As (and also Se) from waters containing dilute concentrations (ppb-level) of these metals. Both uncalcined (as prepared) and calcined (materials that have been heated at temperatures at ~ 500 ^{o}C for a number of hours) LDH adsorbents were investigated. The calcined materials exhibited higher adsorption capacity and efficiency than the uncalcined LDH; this was attributed to the higher surface areas of the former materials, and also because when the calcined LDH are put in contact with anion-containing waters, they rapidly rehydrate and adsorb the anions, in the process reconstructing their original structure.   The adsorption isotherm, kinetics, as well as the effects of the As oxidation state, pH, temperature, and the presence of competing anion on the adsorption were also investigated.

However, in the first part of our study the adsorption data were modeled though a simple empirical exponential rate model, which does not provide significant physical insight into the adsorption of these metals into the LDH. In addition, during the adsorption run the solution pH changed significantly, which adds additional uncertainty in the interpretation of the data. For the calcined materials, in particular, during the batch tests some dissolution of Al and Mg from the LDH structure was observed; and though these metals are not currently regulated, they are bound

to be a source of concern for the eventual use of these materials in drinking water applications.

In further experiments, as a result, our focus shifted on calcined LDH materials which have undergone a conditioning process (see below) prior to their use in the experimental runs. Such conditioning seems to have two beneficial effects. First, it reduces significantly the Al and Mg dissolution, and second it tempers the solution pH change, something that was even a concern with the unconditioned LDH in our preliminary study [Yang *et al*., 2005]. With these materials we have carried a series of studies the goal of which was two-fold: (i) to investigate the effect of an important parameter, namely the adsorbent particle size, a key consideration for the field-testing of these materials in flow columns, where pressure drops and particle carry-over are concerns; and (ii) to develop a more detailed model of the adsorption process, which better relates batch experiments with flow-column runs.

Two models are utilized here to describe the batch experimental data. The first is the classical homogeneous "surface diffusion" model [Tien *et al*., 1994] that has been previously utilized to describe adsorption of metals and other pollutants in nanoporous adsorbents like, for example, sorption of metal cations by hydrous amorphous aluminum, iron, and manganese oxides [Axe and Trivedi, 2002], the adsorption of arsenate into granular ferric hydroxide (GFH) [Badruzzaman *et al*., 2004] and in natural manganese oxide [Ouvrand *et al.,* 2002], and the adsorption of basic dyes in natural clays [El-Geundi, 1991]. The adsorption experimental data, generated with adsorbents of various particle sizes are investigated first using this model, and the effect of particle size on the adsorption characteristics and the intraparticle diffusivity are analyzed and reported here. In addition, we utilize a bidisperse model, which assumes that the

individual adsorbent particles are agglomerates of individual single crystal microparticles. Two

transport processes are described by this model, the first taking place in the porous region in

between the microcrystallites, and the second describing transport within the crystallites

themselves. This latter model is consistent with TEM experimental observations of the particles

themselves, and the presence of a porous region as indicated by the BET measurements.

2.2.3.1 Mathematical models

2.2.3.1.1 The Homogeneous Surface Diffusion Model

As noted above, the homogeneous "surface diffusion" model [Tien, 1994] is used here to describe

the experimental adsorption data. According to this model, the following mass balance equation

describes adsorption in a spherical sorbent particle

$$\frac{\partial q}{\partial t} = \frac{1}{r^2}\frac{\partial}{\partial r}(r^2 D \frac{\partial q}{\partial r}) \tag{4}$$

where q (μg adsorbate/g sorbent) is the adsorbate concentration, r (cm) is the radial distance, and

D (cm^2/s) the intraparticle diffusion coefficient. In general, the diffusivity D of adsorbed

molecules is concentration dependent [Tien, 1994]. In the present study we have fitted this

coefficient by assuming that it is concentration independent, and also concentration dependent

using the classical Darken theory for which the diffusivity is given by

$$D_s = D_{s0}\frac{\partial \ln C}{\partial \ln q} \tag{5}$$

where D_{s0} is the diffusivity at zero loading. For the Sips isotherm (see below) Equation. (5) is

reduced to

$$D_s = \frac{D_{s0}}{n}\left(\frac{1}{1-\dfrac{q}{q_s}}\right) \tag{6}$$

and q_s is the saturation loading. n is the exponential factor in the Sips isotherm.

At the external particle surface (r=R), instantaneous equilibrium is assumed between the liquid and solid phase metal species concentrations, which are coupled using the Sips isotherm equation, as obtained from the isotherm experiments (see further discussion below).

$$q = \frac{Kq_s C_s^{\;n}}{1+KC_s^{\;n}} \qquad \text{r=R} \tag{7}$$

where C_s is the liquid phase concentration (µg/l) at the solid-liquid interface. Equations (8)-(10) below are the other initial (IC) and boundary conditions (BC):

$$q=0, \qquad 0 \le r \le R,\ t=0, \tag{8}$$

$$\frac{\partial q}{\partial r} = 0, \qquad r=0 \tag{9}$$

In the column-flow experiments external mass transfer limitations are often of concern, and the following equation is utilized to describe mass transport from the liquid phase bulk to the particle-liquid interface.

$$\rho D_i \left.\frac{\partial q}{\partial r}\right|_{r=R} = k_f (C - C_s) \qquad \text{r=R} \tag{10}$$

where ρ (g/cm^3) is the particle density, k_f (cm/s) is the external mass transfer coefficient; C (µg/l) is the bulk liquid phase concentration.

In the batch experiment the vials containing the adsorbent and solutions were vigorously agitated in order to eliminate external mass transport limitations; we determined the conditions

for which external mass transfer limitation are no longer important, by varying the rate of agitation and measuring the corresponding rates of adsorption. An agitation speed of 170 rpm was deemed sufficient to eliminate external mass transport limitations, and all batch experiments were, therefore, carried out under such conditions so that $C=C_s$.

Equations. (4) – (10) above must be coupled with the overall mass balance for the batch adsorption vial given by:

$$V(C_0\text{-}C)=M\,\overline{q} \tag{11}$$

where C_0 (μg/l) is the initial liquid phase concentration, V (ml) is the initial volume of solution, M (mg) is the initial adsorbent mass, and $\overline{q}$ ((μg/g)) is the volume-averaged adsorbate concentration in the adsorbent particle defined as:

$$\overline{q} = \frac{3}{R^3}\int_0^R q\,r^2 dr \tag{12}$$

For loading-dependent diffusivity, the Darken Equation (6) has been used instead. To consider particle size distribution (PSD), Equation (4) and Equations (8) – (10) were modified to the following equations:

$$\frac{\partial q_i}{\partial t} = \frac{1}{r_i^{\,2}}\frac{\partial}{\partial r_i}(r_i^{\,2} D \frac{\partial q_i}{\partial r_i}) \tag{13}$$

where i denotes the ith fraction of particle size distribution.

BC and IC are:

$$q_i=0, \qquad t=0, \tag{14}$$

$$\frac{\partial q_i}{\partial r_i} = 0, \qquad r_i=0 \tag{15}$$

$$q_i = \frac{Kq_sC_s^{1/n}}{1 + KC_s^{1/n}}, \qquad r_i = R_i \qquad\qquad (16)$$

$$\overline{q_i} = \frac{3}{R_i^3} \int_o^{R_i} q_i r_i^2 dr_i \qquad\qquad (17)$$

$$\overline{q} = \frac{1}{M} \sum_i M_i \overline{q_i} \qquad\qquad (18)$$

Equations. (13)-(18) together with Equation. (11) are solved to obtain the diffusivity D.

2.2.3.1.2 The Bidisperse Pore Model

In the bidisperse pore model the assumption made is that the adsorbent particle is an agglomerate of a number of equal size, single crystal microparticles. A porous intercrystalline region forms in between the microparticles. Before the metal anion adsorbs inside the microparticle structure, it must be transported from the particle surface, through the inercrystalline region to the surface of the microparticles. In the inercrystalline porous region transport is described by the following equations [Tien, 1994]

$$\frac{\partial C_M}{\partial t} + \frac{(1-\varepsilon)}{(\varepsilon)}\frac{\rho_s \partial \overline{q_\mu}}{\partial t} = \frac{D_M}{r_M^2}\frac{\partial}{\partial r_M}\left[r_M^2 \frac{\partial C_M}{\partial r_M} \right] \qquad\qquad (19)$$

BC and IC are:

$$C_M = 0, \qquad\qquad t = 0 \qquad\qquad (20)$$

$$\frac{\partial C_M}{\partial r_M} = 0, \qquad r_M = 0 \qquad\qquad (21)$$

$$C_M = C(t), \qquad r_M = R_M \qquad\qquad (22)$$

where C_M is the solute concentration in the intercrystalline porous region (μg/l), $\overline{q_\mu}$ is the volume-averaged solute concentration in the solid phase (microparticles) (μg/g) – see Equation

29 below, R_M the particle external radius, and ε is the void fraction in the porous region.

Transport and adsorption in the microparticles are described by

$$\frac{\partial q_\mu}{\partial t} = \frac{D_\mu}{r_\mu^2} \frac{\partial}{\partial r_\mu}\left(r_\mu^2 \frac{\partial q_\mu}{\partial r_\mu} \right) \tag{23}$$

BC and IC are:

$$q_\mu = 0, \qquad\qquad t=0 \tag{24}$$

$$\frac{\partial q_\mu}{\partial r_\mu} = 0, \qquad\qquad r_\mu=0 \tag{25}$$

$$q_\mu = \frac{Kq_s C_M^{\,n}(r_M,t)}{1 + KC_M^{\,n}(r_M,t)}, \quad r_\mu = R_\mu \tag{26}$$

where q_μ is the solute concentration (µg/g) in the microparticle, D_μ (cm^2/s) the microparticle

diffusivity, and R_μ the microparticle radius. The bulk concentration, C, can be found by applying

the following equation, which is Equation 11 modified to account for the presence of a bidisperse

structure:

$$V\,(C_0\text{-}C) = M\,\overline{\overline{q}} \tag{27}$$

where,

$$\overline{\overline{q}} = \frac{3}{\rho R_M^{\,3}} \int_0^{R_M} r_M^{\,2}\left[(1-\varepsilon)\rho_s \overline{q}_\mu + \varepsilon C_M \right] dr_M \tag{28}$$

Equations (19) – (28) above must be solved with $\overline{q}_\mu$ being given by

$$\overline{q}_\mu = \frac{3}{R_\mu^{\,3}} \int_0^{R_\mu} q_\mu r_\mu^{\,2} dr_\mu \tag{29}$$

By defining the following dimensionless variables

$$\eta = \frac{r_M}{R_M} \qquad\qquad \beta = \frac{r_\mu}{R_\mu}$$

$$\overline{C}_M = \frac{C_M}{C_0} \qquad\qquad \overline{C} = \frac{C}{C_0}$$

$$Q_\mu = \frac{q_\mu}{q_s} \qquad\qquad \overline{Q}_\mu = \frac{\overline{q}_\mu}{q_s}$$

$$\overline{\overline{Q}} = \frac{\overline{\overline{q}}}{q_s} \qquad\qquad \tau = t\,\frac{D_M}{R_M^{\,2}}$$

and setting

$$D = \frac{D_M}{R_M^{\,2}} \qquad\qquad \overline{D} = \frac{D_\mu}{R_\mu^{\,2}}$$

$$\alpha = \frac{\overline{D}}{D} \qquad\qquad \Omega = \frac{Mq_s}{VC_0}$$

$$\Lambda = KC_0^{\,n} \qquad\qquad \omega = \frac{\rho_s q_s}{C_0}$$

Equations (19) - (29) above are converted to the following dimensionless equations.

$$\frac{\partial \overline{C}_M}{\partial \tau} + \frac{(1-\varepsilon)}{(\varepsilon)}\omega\frac{\partial \overline{Q}_\mu}{\partial \tau} = \frac{1}{\eta^2}\frac{\partial}{\partial \eta}\left[\eta^2 \frac{\partial \overline{C}_M}{\partial \eta}\right] \qquad\qquad (30)$$

BC and IC:

$$\overline{C}_M = 0, \qquad \tau = 0 \qquad\qquad\qquad (31)$$

$$\frac{\partial \overline{C}_M}{\partial \eta} = 0, \qquad \eta = 0 \qquad\qquad\qquad (32)$$

$$\overline{C}_M = \overline{C}(\tau), \qquad \eta = 1 \qquad\qquad\qquad (33)$$

$$\frac{\partial \overline{Q}_\mu}{\partial \tau} = \frac{\alpha}{\beta^2}\frac{\partial}{\partial \beta}\left(\beta^2 \frac{\partial \overline{Q}_\mu}{\partial \beta}\right) \qquad\qquad (34)$$

BC and IC:

$$Q_\mu = 0, \qquad\qquad \tau = 0 \qquad\qquad (35)$$

$$\frac{\partial Q_\mu}{\partial \eta} = 0, \qquad\qquad \beta = 0 \qquad\qquad (36)$$

$$Q_\mu = \frac{\Lambda \overline{C}_M{}^n(\eta,\tau)}{1 + \Lambda \overline{C}_M{}^n(\eta,\tau)}, \qquad \beta = 1 \qquad\qquad (37)$$

$$\overline{Q}_\mu = 3 \int_0^1 Q_\mu \beta^2 d\beta \qquad\qquad (38)$$

$$(1 - \overline{C}) = \Omega \overline{\overline{Q}} \qquad\qquad (39)$$

where,

$$\overline{\overline{Q}} = \frac{3}{\rho} \int_0^1 \eta^2 \left[(1-\varepsilon)\rho_s \overline{Q}_\mu + \varepsilon \frac{C_0}{q_s} \overline{C}_M \right] d\eta \qquad\qquad (40)$$

The dimensionless equations are solved and fitted to the experimental data to calculate the value

of $\overline{D}$; D_M is taken to be the bulk diffusivity of $H_2AsO_4^-$ in water [Lide, 1996] (this assumption

may not be entirely correct, as diffusion in the porous region may be hindered, and effective

diffusivity may be lower than that in the bulk [Lin and Wu., 2001]; however, relaxing this

assumption will not change the qualitative conclusions using the bidisperse model).

2.2.3.2 Experimental results

The Mg-Al-CO$_3$-LDH utilized in these experiments (with a Mg/Al molar ratio of 2.87) was

prepared by the co-precipitation method. 140 ml of a solution containing 0.7 mol NaOH and 0.18

mol Na$_2$CO$_3$ was added all at once to a second solution containing 0.115 mol of Mg(NO$_3$)$_2$·6H$_2$O

(90ml) and 0.04 mol of Al(NO$_3$)$_3$·9H$_2$O (90 ml) (corresponding to a Mg/Al ratio equal to 2.87)

under vigorous stirring. The thick gel obtained was aged for 24 h at 333 K, followed by filtration

and washing with distilled water, and was then dried at 333 K. ICP-MS analysis of the resulting

LDH material indicated that its Mg/Al mole ratio is ~2.9, very close to the Mg/Al ratio of the starting salts.

The calcined Mg-Al-LDH was obtained by heating the original LDH in a muffle furnace at 773 K for 4 h in an air atmosphere with heating and cooling rates of 2 K·min^{-1}. The calcined LDH was conditioned by shaking it in deionized water for 24 h (changing the deionized water every 6 h), and then drying in air atmosphere at 353 K for 12 h. The conditioned LDH was crushed and sieved using standard testing sieves (VWR) into four different fractions with mesh sizes 200-270 mesh (75-53μm), 170-200 mesh (90-75μm), 80-170 mesh (180-90μm), and 50-80 mesh (300-180μm).

The arsenate solutions used for the adsorption experiments were prepared by dilution from 1000 ppm ICP standard solutions (As(V) in 2 % HNO_3 purchased from Exaxol) using deionized water. No effort was made to minimize contact with the atmospheric air during the preparation of the various solutions. All experiments were carried out in 1000 ml polyethylene bottles at 298K and at 170 rpm. The details of isotherm and kinetic experiments are as follows:

The adsorption isotherm experiments were carried out in 1000 ml polyethylene bottles at a temperature of 298 K using conditioned LDH. 20 mg of the adsorbent were added to 500 ml of an aqueous solution of As(V) of varying concentrations, ranging from 60 ppb to 300 ppb. The initial pH of these solutions was adjusted to ~7.0 using a 0.1M NaOH solution. The bottles containing the LDH suspension and the As(V) solutions were placed in a reciprocal shaking water-bath (Precision Model 25) and were shaken at 170 rpm (rotations per minute) for 5 days in order for the adsorption on the conditioned LDH to reach equilibrium. 5ml samples from each bottle were

taken and centrifuged, and the As concentrations in the supernatant solutions were determined by ICP-MS (Perkin-Elmer ELAN-9000). The instrument detection limit was found to be 0.043 μg/l for As using the EPA 200.8 method.

For the kinetic experiments, As(V) solutions with initial concentration of around 205 ppb were prepared. The initial pH was adjusted to around 7 using NaOH. The pH was not adjusted during the adsorption period. pH changes were measured and recorded using an Accumet Basic AB 15 pH meter. 20 mg of adsorbent mass was added to the 500 ml aqueous solutions in 1000 ml flasks which were then shaken at 170 rpm. At selected time intervals, 5ml samples were extracted, centrifuged, and the As concentrations as well as the dissolved Mg and Al in solution were determined by ICP-MS. The adsorption runs were repeated for the various particle size ranges.

For characterization, scanning electron microscopy (SEM) using a Cambridge 360 SEM instrument (Cambridge Instruments, UK) was used to measure the adsorbent particle sizes. The SEM images were analyzed using the software of ImageJ, in order to obtain the average particle size, and particle size distribution (PSD).

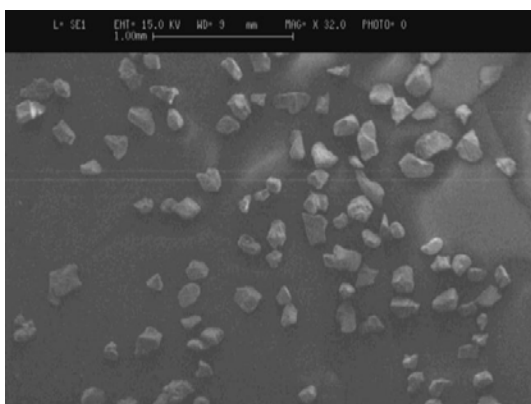**2.2.3.2.1 Particle size distribution**

Figure 10 shows the SEM pictures of the conditioned LDH for the four different particle size ranges. For each particle size, several SEM pictures are taken and are used to determine the PSD of the adsorbent. Representative particle size distribution profiles of the conditioned LDH are shown in Figure 11.
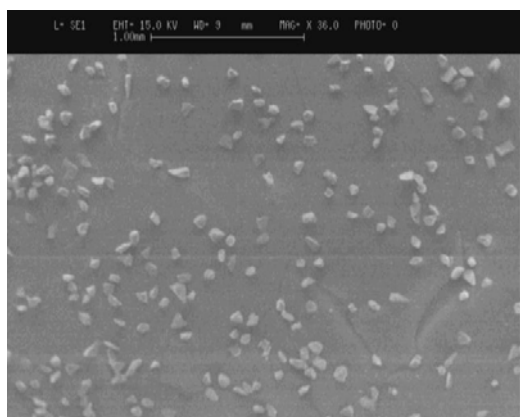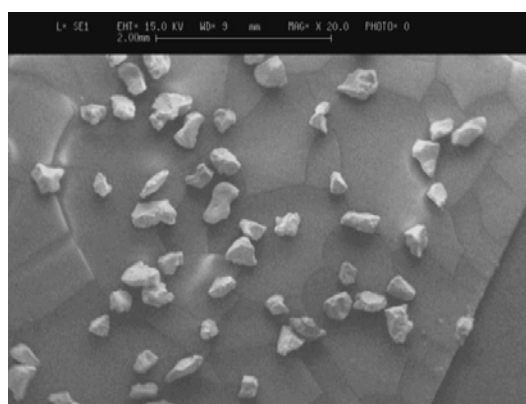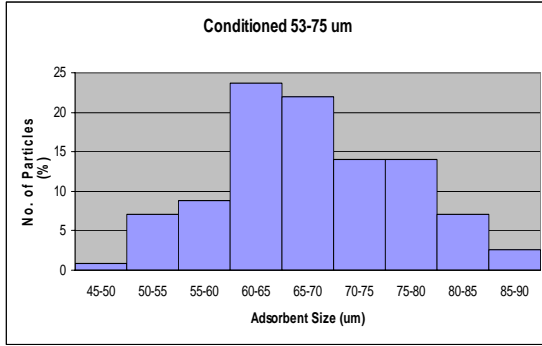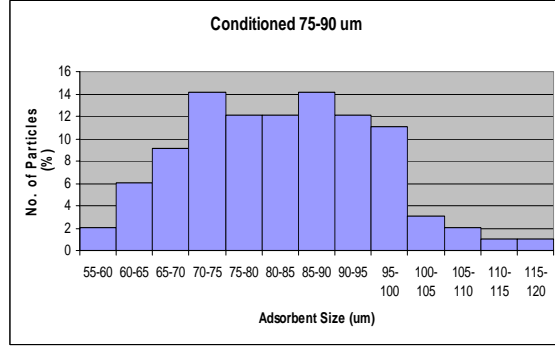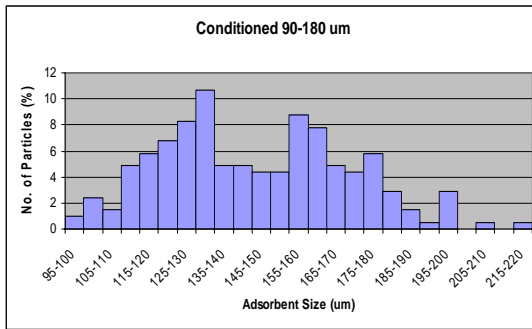
(a)
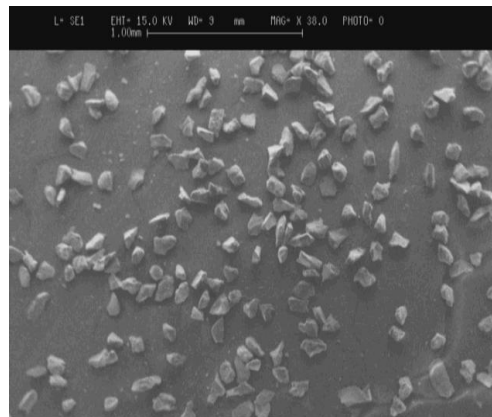
(b)

(c)

(d)

Figure 10 SEM pictures of conditioned LDH with mesh size of (a) 200-270 mesh (75-53μm); (b)

170-200 mesh (90-75μm), (c) 80-170 mesh (180-90μm), and (d) 50-80 mesh (300-180μm)

(a)   (b)
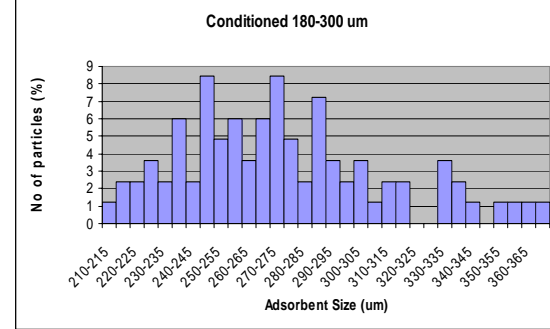

(c)   (d)

Figure 11. Particle size distribution profiles for conditioned LDH.

There are a number of ways to define the average particle-size, characterizing every range.

We utilize here the two most popular definitions [Kaczmarski and Bellot, 2001], namely:

1. The arithmetic mean:

$$d_{10} = \frac{\sum_i n_i d_i}{N} \tag{41}$$

where $N = \sum_i n_i$, i is an index of the population, and d_i is the particle diameter of population i.

2. The volume mean:

$$d_{30} = \left(\frac{\sum_i n_i d_i^3}{N} \right)^{1/3} \tag{42}$$

Fairly similar average particle sizes are obtained (generally d_{30} is somewhat larger than d_{10}) based on these two definitions, and the results (also shown in the table are the fitted diffusivities) are shown in Tables 3 and 4. Table 5 shows the diffusivity values using the bidisperse pore model. Listed in the table are the $\frac{D_\mu}{R_\mu^2}$ values as we cannot accuarately measure the size of the microparticles.

Table 3 Surface diffusion coefficients for various conditioned LDH particle sizes

Mesh size	d_{10} (µm)	D	d_{30} (µm)	D	D^*
		$(\times 10^{11}\ \mathrm{cm^2/s})$		$(\times 10^{11}\ \mathrm{cm^2/s})$	$(\times 10^{11}\ \mathrm{cm^2/s})$
200-270	68.1	1.64249	69.2	1.69598	1.12
170-200	82.7	1.6457	84.6	1.72219	1.02
80-170	146.3	3.90617	150.5	4.13367	2.59
50-80	274.5	10.031	279.4	10.3923	6.47

D* obtained considering particle size distribution

Table 4 D_{s0} for various conditioned LDH particle sizes

| Mesh size	d_{10} (μm)	D_{s0} ($\times 10^{11}$ cm^2/s)	d_{30} (μm)	D_{s0} ($\times 10^{11}$ cm^2/s)
200-270	68.1	0.257279	69.2	0.26565
170-200	82.7	0.260885	84.6	0.27301
80-170	146.3	0.613929	150.5	0.64968
50-80	274.5	1.60609	279.4	1.66394

Table 5 Measured densities and porosities and simulated D_{μ}/R_{μ}^2 for various conditioned LDH

particle sizes

Mesh Size	Density (g/cm^3)	Porosity	D_{μ}/R_{μ}^2 ($\times 10^7$ sec^{-1})
200-270	1.964	0.58	5.01
170-200	1.983	0.53	5.50
80-170	1.975	0.46	5.68
50-80	1.986	0.48	5.82

2.2.3.2.2 Adsorption kinetics and isotherms of As(V) on LDH

Figure 12 shows a typical example of the time dependence of As (V) adsorption on conditioned

LDH (particle size of 75-90μm) with an initial concentration of around 205 μg/l. During the adsorption experiment, the pH in the solution changes gradually from an initial value of 6.7 to a final value of 7.1. The pH increase was also reported by Kang *et al.* [1999] when they investigated the adsorption of I⁻ on Mg/Al layered double hydroxide, and by Seida *et al.* [2001] for the adsorption of dilute lead on pyroaurite-like compound. This pH change for our conditioned LDH is significantly smaller than what is observed with an uncalcined and calcined (but unconditioned) LDH [Yang *et al.*, 2005].
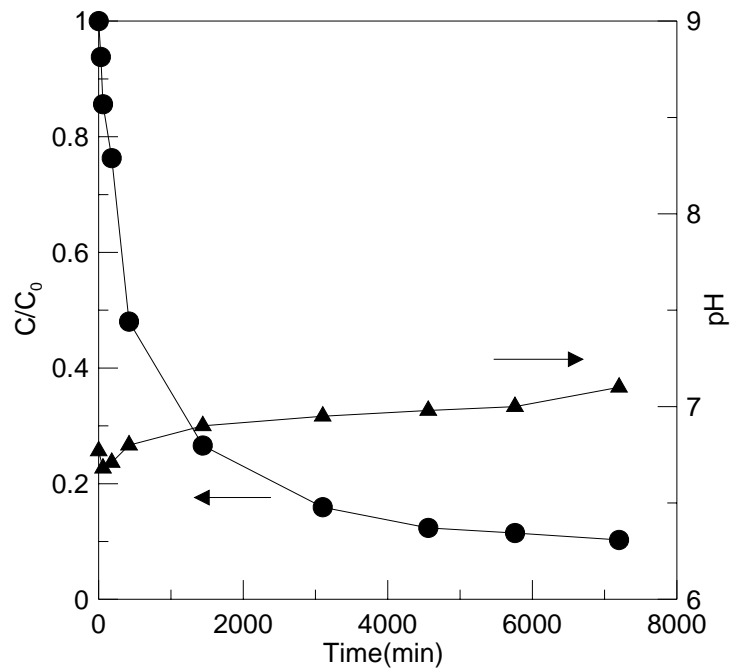
Figure 12. Time dependence of As(V) adsorption on conditioned LDH; particle size of 75-90μm, C_o of 205 μg/l, dose of 0.04g/l.

During the adsorption process there is some dissolution of the conditioned LDH as it is manifested by the presence of Al and Mg in solution, see Figure 13. As shown in Figure 4, the

concentration of Al, as detected by ICP-MS analysis, first increases with time and finally levels

off at 40 ppb; the Mg concentration, on the other hand, gradually increases throughout the whole

experiment. (Independent experiments using Al and Mg soluble salts have shown that the Al and

Mg present have no influence on the As adsorption, and they do not interfere with the ICP/MS

analysis for As).
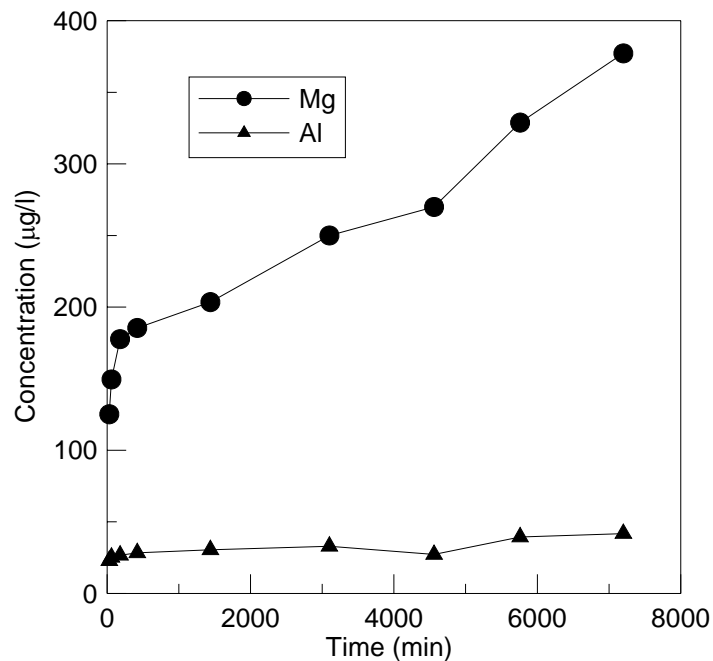
Figure 13. Mg and Al content in the solutions as a function of time during the kinetic runs;

particle size of 75-90μm, C_o of 205 μg/l, dose of 0.04g/l.

Recently, aluminum is attracting attention, because exposure to it is thought of as a potential risk

factor for the development or the acceleration of the onset of Alzheimer disease in humans [WHO

Guidelines, 1998]. Though not currently regulated, the National Secondary Drinking Water

Regulation (NSDWR) for Al stipulates a range of 0.05-0.2 mg/l. The Al levels in Figure 13 are

outside the NSDWR range.

Figure 14 shows the adsorption kinetics of As(V) for an initial solution pH of 6.7 measured with the four different particle size ranges, described above. It reveals that the adsorption rate increases with decreasing particle size of the conditioned LDH. Lazaridis *et al.* [2004] investigated the adsorption of Cd(VI) on Mg-Al-CO₃ hydrotalcite, and also reported that decreasing the size of the sorbent had a significant effect on the sorption rate, but not on the sorption loading. The same appears to be true here for the adsorption of As(V) on the conditioned LDH. The adsorption isotherms of As(V) (at an initial pH of ~6.7) on the conditioned LDH as a function of particle size are shown in Figure 15. There are no significant differences in the isotherms generated with the different particle sizes.
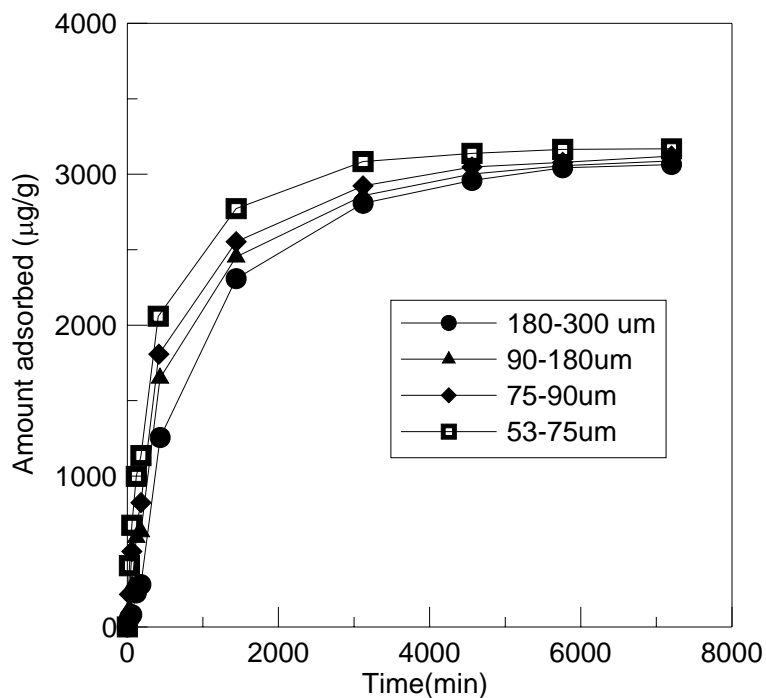
Figure 14. Effect of particle sizes on the adsorption kinetics of As(V) on conditioned LDH.
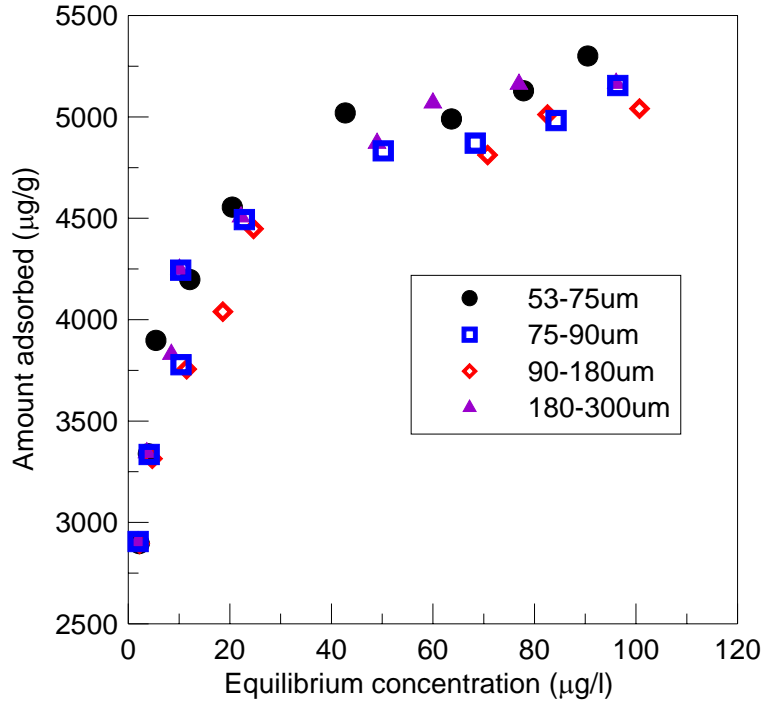
Figure 15. Adsorption isotherm of As (V) on LDH as a function of particle size.

In Figure 16 the data are fitted to Sips isotherm which is given by Eqn. 7. The various

isotherm parameters and the "goodness of fit" as manifested by the R^2 are shown in Table 6.

Table 6. Sorption isotherm parameters for As(V) uptake on conditioned LDH

	Sips Isotherm		
q_s	K_l	N	R^2
$(\mu g/g)$	$(l/\mu g)^n$		
6130.28	0.65478	0.45306	0.95952

The data in Figure 14 are fitted to the "surface diffusion" model, and the fitted lines are

shown in Figure 17 for the different particle sizes. The solid lines correspond to the homogeneous

model with a constant diffusivity, and the particles assumed to be of uniform size with an average diameter equal either to d_{10} or d_{30}. The dashed lines are calculated assuming that the particles are again of uniform size (with an average diameter equal either to d_{10} or d_{30}), but the diffusivity is concentration-dependent, following the Darken correlation. The estimated diffusivity values for the different cases are shown in Tables 3 and 4. For all cases, the diffusivity values are shown to depend on the particle size. For the first case (where the d_{10} is utilized) the D values range from 1.64×10^{-11} cm^2/s to 10.03×10^{-11} cm^2/s and increase with increasing adsorbent particle size For the second case using the d_{30}, the D values range from $1.69x10^{-11}$ cm^2/s to 10.39×10^{-11} cm^2/s. For the case when diffusivity is loading-dependent (see Table 4) the values for D_{s0} (when the d_{10} is utilized) range from 2.57×10^{-12} cm^2/s to 16.06×10^{-12} cm^2/s (for cadmium and copper ion adsorption onto bone char, in contrast, using a concentration-dependent diffusivity resulted in D_{s0} values which do not vary with particle size [Ko *et al*., 2003]). The estimated D values are similar in magnitude to diffusivity values that have been reported for the adsorption of arsenate in granular ferric hydroxide [Badruzzaman *et al*., 2004], as well as cadmium on iron-bearing materials [Smith, 1996]. Axe and Trivedi [2002], for example, investigated intraparticle surface diffusion of metal contaminants in microporous amorphous Al, Fe, and Mn oxides. The surface diffusivities were observed to range from 10^{-16} to 10^{-10} cm^2/s for strontium, cadmium, zinc, and nickel on hydrous amorphous aluminum, iron, and manganese oxides correspondingly. On the other hand, these diffusivities are significantly higher than the values measured during arsenite and arsenate adsorption onto activated alumina [Lin and Wu, 2001] and arsenate onto natural manganese oxide [Ouvrand *et al.,* 2002] (of the order of $\sim10^{-7}$-10^{-8} cm^2/s). They are also higher

than the diffusivities we measure for carbon dioxide in the same materials.
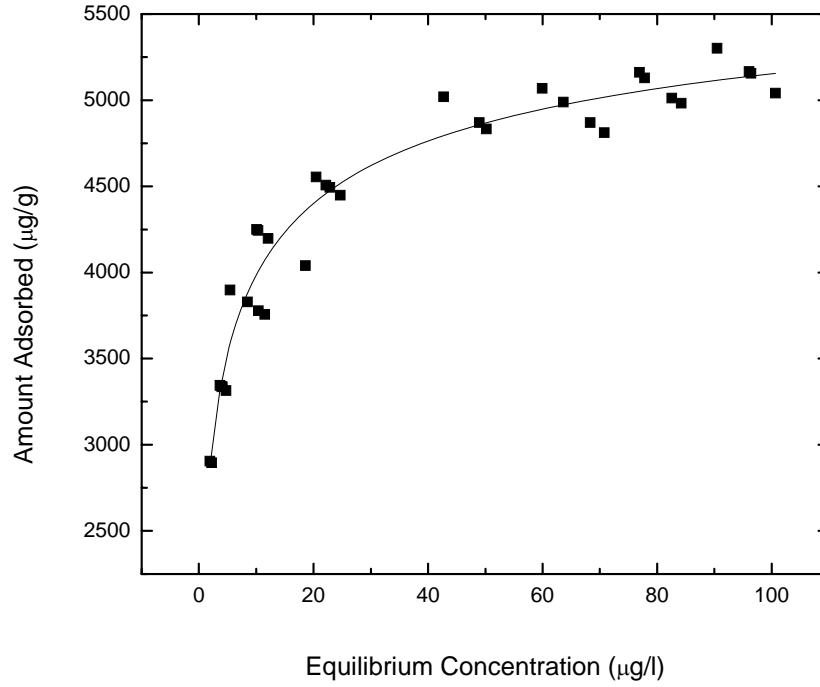
Figure 16. Sips Isotherm model fit for the As adsorption on conditioned LDH.

The strong variation of diffusivity with particle size has also been reported by a number of other investigators. Badruzzaman *et al*. [2004] during adsorption of arsenate in granular ferric hydroxide reported, for example, a non-linear relationship ($D_S=3.0\text{x}10^{-9}Rp^{1.4}$) between D_s and GFH particle radius (R_P). Lin and Wu [2001] reported that during arsenate and arsenite adsorption onto activated alumina the diffusivity also increased with particle size. The same behavior was reported by Ouvrard *et al*. [2002] for arsenate adsorption in natural manganese oxide.
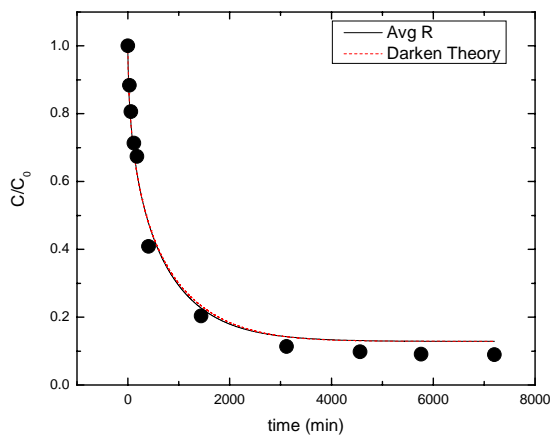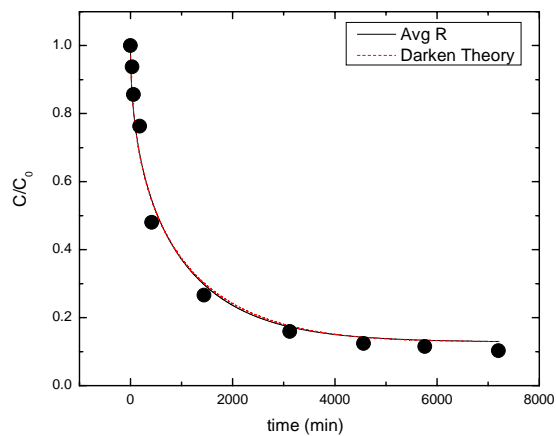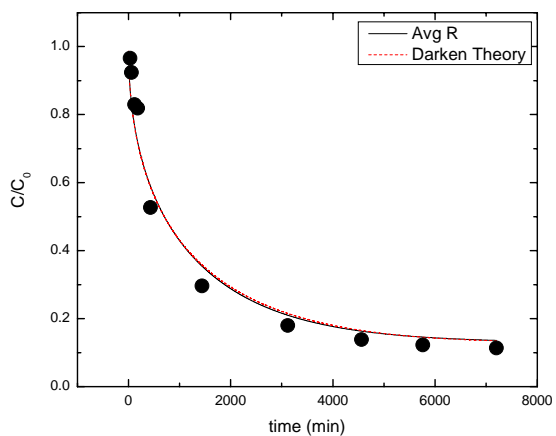
Figure 17 Observed experimental data (symbols) and model predictions (lines) for As(V) adsorption on conditioned LDH with various particle size: (a) 53-75 μm; (b) 75-90 μm; (c) 90-180 μm; (d) 180-300 μm. Solid line denotes simulated uptake curves for d_{10} and d_{30}, and the dash line denotes simulated uptake curves calculated loading dependent diffusivity.

On the other hand, the opposite trend was observed during adsorption of cadmium on

iron-bearing materials derived from surface finishing operations in the manufacturing of cast iron components [Smith, 1996]. To verify whether this particle size dependence on diffusivity is the result of using an average particle size rather than the experimental particle size (approximation of the PSD by use of an average diameter has been shown in the past to lead to misinterpretation of the experimental data [Kaczmarski and Bellot, 2003]), the data were also fitted using Eqns (13)-(18) above and the experimentally measured particle size distribution. Despite taking into account the particle size distribution, the estimated D values are still particle size dependent, and range from 1.12×10^{-11} cm^2/s to 6.47×10^{-11} cm^2/s.

Finally, the experimental data were also fitted to the bidisperse pore model described by Equations (30) – (40) above. Since we do not have accurate experimental data on the radius of the single crystal microparticles constituting the larger particle, we opted instead to estimate the values of $\dfrac{D_\mu}{R_\mu{}^2}$ (in s^{-1}). The diffusivity of the metal anions in the porous region was taken to be equal to its bulk diffusivity value, which has already been reported in the technical literature [Lide, 1996]. The $\dfrac{D_\mu}{R_\mu{}^2}$ values are reported in Table 5 and the data and parameter fit are shown in Figure 18. Note, that though there is still some variation with respect to particle size, it is significantly less than that in the estimated diffusivity values from the homogeneous model. This observation is consistent with the understanding that the surface diffusivity within the microparticles should
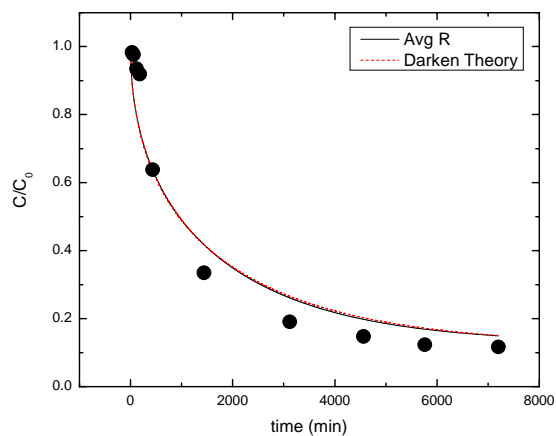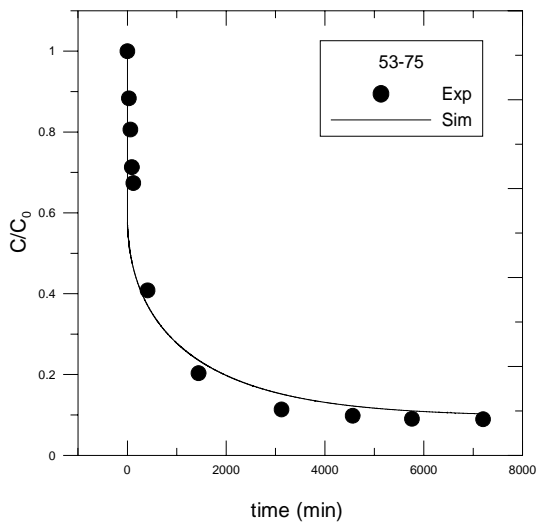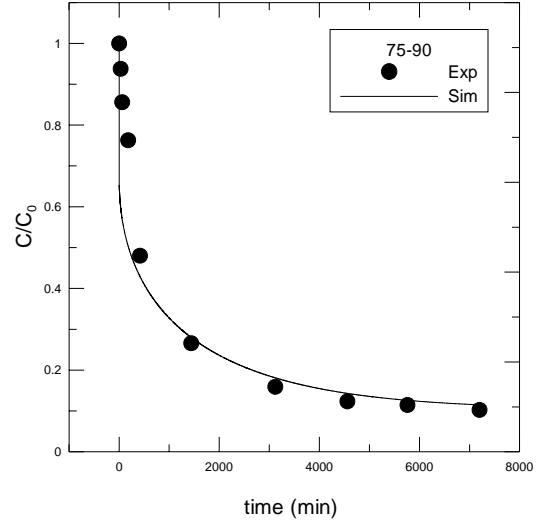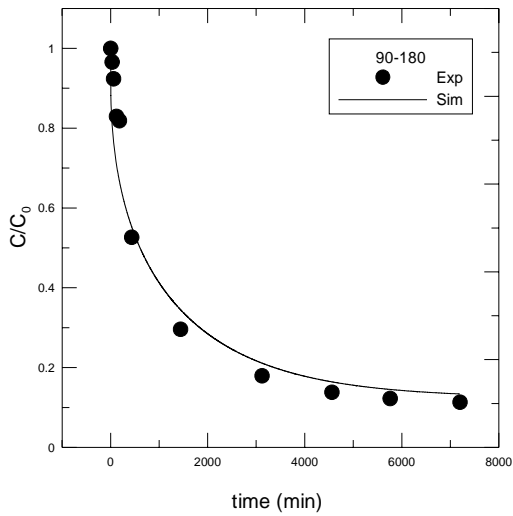
Figure 18 Observed experimental data (symbols) and model predictions (lines) for As(V) adsorption on conditioned LDH with various particle size: (a) 53-75 μm; (b) 75-90 μm; (c) 90-180 μm; (d) 180-300 μm. Solid line denote simulated uptake curves using bidisperse pore model

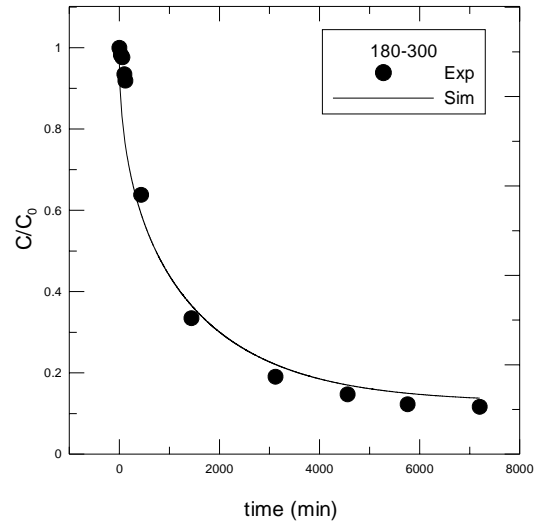remain unaffected by the overall size of the aggregate particle. Given the uncertainty in the assumption that the microparticles are all of uniform size, it is probably safe to say that the bidisperse model offers a more accurate representation of the transport and adsorption processes that take place, and it should be more appropriate to utilize in flow experiments with these materials, in lieu of the commonly utilized homogeneous surface diffusion model.

2.2.4. Model development for packed-bed flow adsorption columns.

The design of industrial adsorption columns requires substantial quantities of information. Typically, all such design information is gathered in an extensive series of pilot-plant experiments that are time-consuming and expensive. As part of this project, a model has been developed, which is applicable to the design of such industrial systems; the plan during phase II of this project is to validate the model by bench-scale experiments. Once validated, this model will be utilized in the design of a full-scale column to study the effect of the various operating parameters. These parameters include linear flow rate, feed concentration, pH, and temperature. With variation of the above parameters, the optimum conditions for the column operation can be predicted. This model allows one to successfully study the column dynamics and breakthrough curves for a specific set of operating conditions.

In the model mass transport in the adsorbent particles is described either by the homogeneous surface diffusion or the bidisperse model. For the homogeneous surface diffusion model, for example, mass transport is described by the following unsteady state equations:

$$\frac{\partial q}{\partial t} = \frac{D}{r^2}\frac{\partial}{\partial r}(r^2\frac{\partial q}{\partial r}) \qquad\qquad (43)$$

Equation (43) must be solved with appropriate initial and boundary conditions:

$$q = 0, \qquad 0 \leq r \leq R, \ t = 0, \tag{44}$$

$$\frac{\partial q}{\partial r} = 0, \qquad r = 0 \tag{45}$$

$$\rho D \left. \frac{\partial q}{\partial r} \right|_{r=R} = k_f (C - C_s) \qquad r = R \tag{46}$$

where ρ (g/cm^3) is the adsorbent density, K_f (cm/s) the mass transfer coefficient, C (g/l) the

concentration of the metal in the liquid, and C_s the metal concentration at the particle interface.

Adsorption equilibrium prevails at the interface, and

$$q = \frac{K q_s C_s^{\,n}}{1 + K C_s^{\,n}} \qquad \text{at } r = R \tag{47}$$

The average concentration throughout the adsorbent particle is defined as:

$$\bar{q} = \frac{3}{R^3} \int_0^R q \ r^2 dr \tag{48}$$

The mass balance in a packed tube reactor for non-dispersive conditions is described as;

$$u \frac{\partial C}{\partial z} + \varepsilon \frac{\partial C}{\partial t} + (1 - \varepsilon) \frac{\partial \bar{q}}{\partial t} \cdot \rho = 0 \tag{49}$$

where u (cm/s) is the average superficial (i.e., calculated in terms of the cross-sectional area of

the column) velocity of the flowing fluid, t (s) is the time, z (cm) the axial distance coordinate,

and ε the void fraction in the bed (in practice, of interest is the number of bed volumes that can be

treated before adsorbent saturation is reached; this can be conveniently calculated from the model

by multiplying the volumetric flowrate with the time needed to reach saturation and by dividing

by the bed volume).

Initial and boundary conditions can be described as,

$$C=0, \text{ at } t=0; \hspace{4cm} (50)$$

$$\bar{q}=0, \text{ at } t=0; \hspace{4cm} (51)$$

$$C=C_0, \text{ at } z=0; \hspace{4cm} (52)$$

In the model the D and K values are obtained from the batch experiments described above, and literature formulas are used to calculate k_f. In the bench-scale column experiments we will study the effect of initial As and Se concentration and the effect of flow-rate on breakthrough behavior.

3. Conclusions

The following discussion summarizes some of our significant accomplishments and findings during the project:

- The As and Se concentrations in power plant effluent streams were determined. Typical contaminant profiles of such streams were established, and "surrogate" boiler blow-down streams were created to perform preliminary reclaim/reuse studies focusing on calcined and uncalcined layered double hydroxides.

- The removal of As and Se from model boiler blow-down streams on calcined and uncalcined layered double hydroxides was studied**.** The following represent some of the key observations and findings of this Task:

  1. The LDH materials have been well-characterized by a variety of techniques, including in situ DRIFTS and surface area measurements. These structural characterizations provide a better insight into the mechanism of how these materials work in removing metal

anions for polluted wastewaters.

2. Adsorption isotherm experiments indicate that calcined Mg-Al-CO$_3$-LDH is a promising adsorbent for the removal of trace levels of As and Se from aqueous solutions.

3. Empirical exponential rate models provide a satisfactory fit for the adsorption of both As and Se on calcined or on uncalcined LDH.

4. Calcined LDH can be used effectively in a broad pH range (pH above 4).

5. As(III) is more difficult to remove As(V). Therefore, one must first oxidize As (III) to As(V) before using LDH for its adsorption.

6. Competing anions in solution have generally a minimal effect on As and Se adsorption.

- Research was carried out to understand what determines sorbent selectivity. In particular the emphasis was on the effect of adsorbent particle size, as it is critical in determining column performance. Conditioning the adsorbent significantly reduced the dissolution previously observed with uncalcined and calcined (but unconditioned) LDH. The adsorption rates and isotherms have been investigated in batch experiments. The As(V) adsorption rate on conditioned LDH increases with decreasing adsorbent particle size; the adsorption capacity of As(V) on conditioned LDH, on the other hand, is independent of particle size. A homogenous surface diffusion model is used to describe the experimental kinetic data. The estimated diffusivity values are shown to depend on the particle size. When a bidisperse model is used, instead, to describe the same data the estimated diffusivities are particle size independent..

4. Technology Transfer Activities Accomplished during the Project

A technical paper describing our findings was presented at the Annual American Institute of

Chemical Engineers meeting, in Austin, TX in November, 2004. The following technical paper was published in Ind. Eng. Chem Res.

Yang, L., Shahrivari, Z., Liu, P.K.T., Sahimi, M., Tsotsis, T.T. "Removal of Trace Levels of Arsenic and Selenium from Aqueous Solutions by Calcined and Uncalcined Layered Double Hydroxides (LDH)", *Ind. Eng. Chem. Res*., 44, 6804, 2005.

The following paper has been submitted for publication.

Yang, L., Dadwhal M., Shahrivari, Z., Ostwal, M., Liu, P.K.T., Sahimi, M., Tsotsis, T.T. "Adsorption of Arsenic on Layered Double Hydroxides (LDH): Effect of Particle Size," Submitted *Ind. Eng. Chem. Res*.

5. References and Bibliography

- Axe, L.; Trivedi, P. Intrapartilce Surface Diffusion of Metal Contaminants and their Attenuation in Microporous Amorphous Al, Fe, and Mn oxides. *J. Colloid Interf. Sci*. **2002**, 247(2), 259.

- Badruzzaman, M; Westerhoff, P; Knappe, D. R. U. Intraparticle diffusion and adsorption of arsenate onto granular ferric hydroxide., *Water Research*, **2004**, *38*, 4002.

- Basu, A.; Mahata, J.; Gupta, S.; Giri, A. K. Genetic Toxicology of a Paradoxal Human Carcinogen, Arsenic: A Review. *Mutat. Res.* **2001**, *488 (2)*, 171.

- Cavani, F.; Trifiro, F.; Vaccari, A. Hydrotalcite-type Anionic Clays: Preparation, Properties and Applications. *Catal. Today* **1991**, 11, 173.

- Das, D. P.; Das, J.; Parida, K. Physicochemical Characterization and Adsorption Behavior of Calcined Zn/Al Hydrotalcite-like Compound (HTLs) towards Removal of Fluoride

from Aqueous Solution. *J. Colloid Inter. Sci.* **2003**, 261, 213.

- El-Geundi M.S.; Homogeneous Surface Diffusion Model for the Adsorption of Basic Dyestuffs onto Natural Clay in Batch Adsorbers. *Adsor. Sci. Technol.* **1991**, 8, 217.

- Goswamee, R.L.; Sengupta, P.; Bhattacharyya, K.G.; Dutta, D. K. Adsorption of Cr (VI) in Layered Double Hydroxides. *Appl. Clay Sci.* **1998**, 13, 21.

- Guidelines for Drinking Water Quality, 2nd edition, Addendum to volume 1, Recommendations (1998) World Health Organization, Geneva, 3-4.

- Jules, C. A. A. Roelofs; Jeroen, A. van Bokhoven; A. Jos van Dillen; John W. Geus; Krijn P. de Jong. The Thermal Decomposition of Mg-Al Hydrotalcites: Effects of Interlayer Anions and Characteristics of the Final Structure. *Chem. Eur. J.* **2002**, 8 (24), 5571.

- Kaczmarski, K; Bellot, J. Ch. Effect of Particle-Size Distribution and Particle Porosity Changes on Mass-Transfer Kinetics. *Acta Chromatographica*. **2003**, *13*, 22-37.

- Kang, M.J.; Chun, K.S.; Rhee, S.W.; Do, Y. Comparison of Sorption Behavior of I^- and TcO_4^- on Mg/Al Layered Double Hydroxide. *Radiochim. Acta* **1999**, 85, 57,.

- Ko, D.C.K.; Porter, F.F.; McKay G. Effect of Concentration-Dependent Surface Diffusivity on Simulations of Fixed Bed Sorption Systems. *Trans IChemE.* **2003**, *81A*, 1323.

- Kuan, W.-H.; Lo, S.-L.; Wang, M. K.; Lin, C.F. Removal of Se (IV) and Se (VI) from Water by Aluminum-Oxide-Coated Sand. *Wat. Res.* **1998**, 32 (3), 915.

- Lazaridis, N.K.; Pandi, T. A.; Matis, K.A. Chromium(VI) Removal from Aqueous Solutions by $Mg-Al-CO_3$ Hydrotalcite: Sorption-Desorption Kinetics and Equilibrium Studies. *Ind. Eng. Chem. Res*. **2004**, 43, 2209.

- Lide, D.R; Hanbook of chemistry and physics. 77th Edition, **1996-1997**, 5-99.

- Lin T.F.; Wu, J.K.. Adsoprtion of Arsenite and Arsenate within Activated Alumina Grains. Equilibrium and Kinetics. *Wat. Res.* **2001**, *35*, 2049.

- Manju, G. N.; Gigi, M. C.; Anirudhan, T. S. Hydrotalcite as Adsorbent for the Removal of Chromium (VI) from Aqueous Media: Equilibrium Studies. *Ind. J. Chem. Technol.* 1999, 6, 134.

- Masscheleyn, P. H.; Delaune, R. D.; Patrick, W. H. Jr. Arsenic and Selenium Chemistry as Affected by Sediment Redox Potential and pH. *J. Environ. Qual.* **1991**, *20(3)*, 522.

- Ouvrand, S.; Simonnot, M.O.; de Donato P.; Sardin, M. Diffusion-Controlled Adsorption of Arsenate on a Natural Manganese Oxide, *Ind. Eng. Chem. Res.* **2002**, *41*, 6194.

- Reichle, W. T. Synthesis of Anionic Clay-Minerals (Mixed Metal-Hydroxides, Hydrotalcite), *Solid State Ionics* **1986**, 22 (1), 135.

- Saviz, M.; David, C. Application of Activated Alumina for the removal of Selenium from Water. Proceedings-Technical Seminar on Chemical Spills, 15th, Edmonton, Alberta, June 8-9, 1998.

- Seida, Y.; Nakano, Y.; Nakamura, Y. Rapid Removal of Dilute Lead from Water by Pyroaurite-like Compound. *Wat. Res*. **2001**, 35, 2341.

- Smedley, P. L.; Kinniburgh D. G. A Review of the Source, Behavior and Distribution of Arsenic in Natural Waters. *Applied Geochemistry.* **2002**, *17*, 517.

- Smith, E.H. Uptake of Heavy Metals in Batch Systems by a Recycled Iron-Bearing Material. *Wat. Res*., **1996**, 30(10), 2424,

- Steinberger, A.; Stein, E. D. Characteristics of Effluents from Power Plant Generating Stations in the Southern California Bight in 2000. in S. Weisberg and D. Elmore (eds.), Southern California Coastal Water Research Project Annual Report 2004, Westminster, CA.

- Tien, C. Adsorption Calculations and Modeling. Butterworth-Heinemann, Boston, 1994.

- Thirunavukkarasu, O. S.; Viraraghavan, T.; Subramanian, K. S. Arsenic Removal from Drinking Water Using Iron Oxide-Coated Sand. *Water Air Soil Pol.*, **2003**, 142, 95.

- Thirunavukkarasu, O. S.; Viraraghavan, T.; Subramanian, K. S. Removal of Arsenic in Drinking Water by Iron Oxide-Coated Sand and Ferrihydrite-Batch Studies. *Water Qual. Res. J. Can.* **2001**, 36, 55.

- Yang, L.; Shahrivari, Z.; Liu P.K.T.; Sahimi, M.; Tsotsis, T.T. Aqueous Solutions by Calcined and Uncalcined Layered Double Hydroxides (LDH). *Ind. Eng. Chem. Eng.* **2005**, *44*, 6804.

6.   List of Symbols and Acronyms

C   bulk liquid phase concentration, (μg/l)

$\overline{C}$ dimensionless bulk liquid phase concentration

C_M solute concentration in the intercrystalline pore space, (μg/l)

$\overline{C}_M$ dimensionless solute concentration in the intercrystalline pore space

C_0 initial liquid phase concentration, (μg/l)

C_s liquid phase concentration at the solid-liquid interface, (μg/l)

D_M mesopore diffusivity, (cm^2/s)

D_μ micropore diffusivity, (cm^2/s)

D_s intraparticle diffusion coefficient, (cm^2/s)

D_{s0} diffusivity at zero loading, (cm^2/s)

D diffusion time constant in porous region, equal to $\dfrac{D_M}{R_M^2}$

$\overline{D}$ diffusion time constant in the microparticles, equal to $\dfrac{D_\mu}{R_\mu^2}$

K Sips constant

k_f external mass transfer coefficient, (cm/s)

M initial adsorbent mass, (mg)

n exponential factor in the Sips-type isotherm

q solute concentration in the solid phase, $(\mu g/g)$

$\overline{q}$ volume-averaged adsorbate concentration in the adsorbent particle, $(\mu g/g)$

q_μ solute concentration in the microsphere, $(\mu g/g)$

$\overline{q}_\mu$ volume-averaged adsorbate concentration in the microsphere, $(\mu g/g)$

q_s saturation loading, $(\mu g/g)$

Q_μ dimensionless adsorbate concentration in the microsphere

$\overline{Q}_\mu$ dimensionless volume-averaged adsorbate concentration in the microsphere

$\overline{\overline{q}}$ volume averaged adsorbate concentration in the whole particle (pores + microparticles),

$(\mu g/g)$

$\overline{\overline{Q}}$ dimensionless volume averaged adsorbate concentration in the whole particle

(pores + microparticles)

| r | radial distance in particle, (cm) |

| R | particle radius, (cm) |

| r_M | radial distance in particle, (cm) |

| R_M | particle radius in the bidisperse model, (cm) |

| r_μ | radial distance in microparticle, (cm) |

| R_μ | microparticle radius, (cm) |

| t | time, (s) |

| V | initial volume of solution, (ml) |

Subscripts

| 0 | intial conditions |

| i | i^{th} fraction of particle size distribution corresponding to particles of average radius R_i. |

| M | particle |

| μ | microparticle |

| s | saturation condition |

Greek Symbols

| β | dimensionless microparticle radius |

| ε | void fraction in the porous region. |

| η | dimensionless partilce radius |

| τ | dimensionless time |

| α | dimensionless group, equal to $\dfrac{\overline{D}}{D}$ |

Λ dimensionless Sips constant, equal to $KC_0^{\,n}$

ρ particle density, (g/cm^3)

ρ_s solid density, (g/cm^3)

ϕ_i mass fraction of particles with average radius equal to R_i

ω dimensionless group, equal to $\dfrac{\rho_s q_s}{C_0}$

Ω dimensionless group, equal to $\dfrac{Mq_s}{VC_0}$

Acronyms

DRIFTS Diffuse Reflectance Infrared Spectroscopy

DWP Department of Water and Power

EPA Environmental Protection Agency

GCSC Gas Company of Southern California

GFH Granular Ferric Hydroxide

ICP-MS Inductively Coupled Plasma – Mass Spectroscopy

LDH Layered Double Hydroxide

MCL Maximum Contaminant Level

M&PT Media & Process Technology

NSDWR National Secondary Drinking Water Regulation

PSD Particle Size Distribution

RWB Regional Water Board

SCCWPR Southern California Coastal Water Research Project

SEM   Scanning Electron Microscopy

USC   University of Southern California

WHO   World Health Organization